THE UNIVERSITY OF MANITOBA

POSITRON ANNIHILATION IN ORGANIC LIQUIDS AND THE BUBBLE MODEL

by

JAMES STEPHEN KLASSEN

A THESIS

SUBMITTED TO THE FACULTY OF GRADUATE STUDIES

IN PARTIAL FULFILMENT OF THE REQUIREMENTS FOR THE DEGREE

OF MASTER OF SCIENCE

DEPARTMENT OF PHYSICS

WINNIPEG, MANITOBA

October 1976

"POSITRON ANNIHILATION IN ORGANIC LIQUIDS AND THE BUBBLE MODEL"

by

JAMES STEPHEN KLASSEN

A dissertation submitted to the Faculty of Graduate Studies of the University of Manitoba in partial fulfillment of the requirements of the degree of

MASTER OF SCIENCE

DEDICATION

To my wife Cathrine

ACKNOWLEDGEMENTS

The author would like to express his sincere gratitude to Dr. D. P. Kerr for his constant encouragement and assistance in this undertaking.

Acknowledgement and appreciation is due to Dr. S. Dannefaer for his valuable participation in discussions which have hence enlightened this research endeavour.

ABSTRACT

The behavior of the positronium atom in organic liquids has been investigated. Measurement of the Doppler broadened spectra of annihilation photons is shown to be a valid experimental technique in this study. Doppler broadening measurements yielding three Gaussian components are supplemented with lifetime measurements yielding three exponential components. The theory of the bubble model is developed in detail and is applied to the low momentum Doppler component and to the ortho-positronium pickoff rate from the lifetime distribution. Comparison of bubble radii and positronium centre of mass momenta calculated when the bubble model is applied to both the Doppler and lifetime results suggests that a bound state of positronium other than the ground state in the bubble also exists. Measurement of intensities of the various Doppler and lifetime components indicate that $I_1 > I_A > I_3/3$, where I_1 is the shortest lifetime component intensity, I_3 the longest lifetime component intensity and I_A the low momentum component intensity. Several models are considered to explain this result, with the only successful model predicting, as in the bubble model case, the presence of a second bound state of positronium (probably a 2s bubble state of positronium) in the organic liquids investigated.

TABLE OF CONTENTS

CHAPTER		PAGE
	Acknowledgements	iii
	Abstract	iv
	Table of Contents	v
	List of Tables	vii
	List of Figures	viii
I	INTRODUCTION	1
	1.1 General	1
	1.2 Some Pertinent Facts About Positrons	2
	1.3 The Fate of the Positron in Matter	3
	1.4 The Annihilation of Non-Positronium Positrons	4
	1.5 The Formation and Annihilation of Positronium	6
	1.6 Experimental Methods	9
II	THE THEORY OF THE BUBBLE MODEL	12
	2.1 Introduction	12
	2.2 Quantum Mechanical Treatment	14
	2.3 Application to Doppler Spectra	22
	2.4 Application to Lifetime Spectra	27
	2.5 The Bubble Model and Surface Tension	29

III. EXPERIMENTAL METHODS 32

3.1 The Doppler Experiment 32

3.2 The Lifetime Experiment 38

3.3 Source Construction 42

3.4 Sample Degassing 45

3.5 The Choice of Samples 48

IV. RESULTS AND DISCUSSION 50

4.1 The Doppler Spectra 50

4.2 The Lifetime Spectra 56

4.3 Doppler Spectra and the Bubble Model 59

4.4 The Bubble Model and the Lifetime Spectra 63

4.5 Comparison of the Bubble Model Applications 66

4.6 Relationships Between the Various Component Intensities 74

4.7 The "Transition" Model 78

4.8 The "Conversion" Model 81

4.9 The "Branch" Model 85

4.10 Conclusion 92

REFERENCES 93

APPENDIX I: A Test Spectrum Generating Computer Program 95

APPENDIX II: A Least Squares Fit Computer Program 100

APPENDIX III: The Bisection Method 102

LIST OF TABLES

TABLE		PAGE
3.1	The Samples Used	49
4.1	Results for the Doppler Spectra	54
4.2	Results for the Lifetime Spectra	58
4.3	Results of the Theoretical Fit to the Low Momentum Component	61
4.4	Bubble Model Parameters From The Lifetime Results	65
4.5	Comparison of Bubble Model Parameters .	67
4.6	Excited State Parameters	72
4.7	Proportions of 1s and 2s States	73
4.8	Relationships Among Various Intensities	77
4.9	Calculated Results of the "Conversion" Model	84
4.10	Calculations for the "Branch" Model ...	88
4.11	The 2s Bubble State and the Branch Model	91

LIST OF FIGURES

FIGURE		PAGE
2.1	Illustration of Momentum Conservation upon Positron-electron Pair Annihilation	25
2.2	Illustration of Two Ways to Integrate the Momentum Density over a Plane in Momentum Space	26
3.1	Block Diagram for Doppler Set-up	36
3.2	The Resolution Spectrum of ^{85}Sr	37
3.3	Block Diagram for Lifetime Set-up	41
3.4	Construction of Radioactive Source and Sample Tube	47
4.1	Deconvolution of a Doppler Spectrum ..	53
4.2	Total Momentum Distributions in a) Benzene b) Hexane c) 1-Fluorohexane	55
4.3	The Lifetime Spectrum of Hexane	57
4.4	Theoretical and Experimental Momentum Distributions for p-Ps	62

Chapter I

INTRODUCTION

1.1 General

The study of the behaviour of positrons in matter has been the object of research for many years. These studies have established relationships between the measureable properties of the annihilation process and the nature of the physical and chemical environment of the positron just before annihilation. Many theories have been developed to explain these processes. Even though some of these theories may need refinement or further development, the positron is now used as a probe to provide information on properties of the materials in which the positron annihilates.

The reasons for the positron's usefulness as a probe are primarily three-fold. First, due to its mass and charge, the positron is able to penetrate a sample and become a member of its electronic system. Second, the positron is able to send back information to the observer by means of its positron-electron annihilation gamma rays. Third, the positron is able to form a positron-electron atom, positronium, which, unlike the free positron is able to sense its evironment without changing it as significantly as the free positron (e.g. by way of polarization). However, in this case direct information about the medium can be obtained only to the extent that the positronium behaviour depends on its environment rather than upon its internal properties.

1.2 Some Pertinent Facts About Positrons

Like an electron, the positron has a spin of 1/2 ħ, belongs to the class of leptons and obeys the Fermi-Dirace statistics. The positron is usually formed in the radioactive decay of nuclides whose proton to neutron ratio is greater than unity. In matter the positron will annihilate with an electron and the number and energy of photons emitted by positron-electron annihilation are determined by the relative orientation of spins of the positron and electron at the instant of annihilation. If the positron-electron spin system has antiparallel spins, i.e. is a singlet system with total spin, $J = 0$, then the selection rules for the conservation of energy, momentum, and parity require the emission of an even number of γ quanta the most probable being 2 quanta. The separation angle between the two photons will be 180° and the energy of each photon will be .511 MeV provided that the momentum of the electron-positron system is zero upon annihilation. If the positron-electron system has parallel spins, i.e. is a triplet system with total spin, $J = 1$, then the selection rules can be satisfied only by the emission of an odd number of photons. In this case, the probability of more than 3 photons being emitted is very small. Single photon annihilation requires the presence of an external field, and is not significant here. The ratio of the cross-sections for singlet and triplet annihilations is 372:1 for randomly-oriented spins.

1.3 The Fate of the Positron in Matter

In practice, positrons are injected into a medium with an initial kinetic energy much greater than thermal energy, kT. The positron will slow down very rapidly due to collisions. Once slowed down below 100 eV, the positron may be involved in elastic collisions with or without spin flip, excitation and ionization of atoms of the medium, polarization of the medium and the formation of different types of bound states. Ultimately, the positron must annihilate with an electron which it may do either as a free positron or as a positron in a bound state. It is generally assumed that the positron achieves near thermalization in liquids before annihilation. [33A,34]

Two different types of bound states are of special interest. The first type is positronium (abbreviated Ps), consisting of one positron and one electron. (Other more complex bound systems of positrons and electrons such as Ps^- will not be considered here.) The second type of bound system consists of the positron and an ion or molecule of the medium. Bound states of positronium with ions or molecules of the medium are included in this category. Annihilation of non-Ps positrons and the formation and annihilation of Ps are of particular interest and are discussed in some detail in succeeding sections.

1.4 The Annihilation of Non-Positronium Positrons

In dense substances, positrons are stopped in times small compared to their lifetimes. Those positrons which do not form positronium annihilate with electrons bound in the molecules of the medium. Cova and Zappa[2] have measured the number of electrons per atom in condensed materials effective for annihilation in the case of non-positronium positrons. They show that the relation

$$(1) \qquad \lambda = \pi r_0^2 c n_e$$

well describes their results. Here λ is the annihilation rate of free positrons (or the reciprocal of the mean positron lifetime), r_0, the classical electron radius, c, the speed of light and n_e, the effective number of electrons per unit volume. In the above formulation, the result is that each atom contributes approximately the same amount towards n_e, regardless of the structure of the compound in which it exists.

Although a semi-empirical formula such as the one above well describes the annihilation rate of non-positronium postrons in most molecular materials, it has still not been determined whether the positron really annihilates in flight as a free positron. The various avenues that a non-positronium positron could follow prior to its annihilation with an electron may be placed in the following three categories.[1] They are

1) Annihilation in flight as a free positron.

2) Formation of bound states of positrons with molecules of the medium.

3) Other more weakly bound states such as resonance scattering states or polaron states.

The area of the behaviour of non-positronium positrons is thus open to more research and development of theory.

1.5 The Formation and Annihilation of Positronium

When positronium is formed, 1/4 of the yield will be singlet positronium (referred to as parapositronium, or p-Ps) and 3/4 will be triplet positronium (referred to as orthopositronium or o-Ps). This is a result of quantum statistics: p-Ps has one spin state, while o-Ps has three spin states. The lifetimes of p-Ps and o-Ps in vacuum have theoretically been calculated to be 0.125 and 140 nsec, respectively.

There are currently two basically different models which attempt to describe the formation of Ps. In the Ore gap model[3] Ps is formed within a narrow range of energies called the Ore gap. If the molecules of the medium have an ionization potential V, then, since the positron-electron binding energy in the Ps atom ground state is 6.8 eV, positronium formation is an endothermic reaction with a threshold energy of (V-6.8) eV. For positron kinetic energies above V, ionization of the molecules of the medium becomes more probable than the formation of positronium. In some cases, the upper limit to positronium formation has been taken to be E_1, the first excitation energy of the molecules. The positronium formation probability, P, is taken to be equal to the ratio of the Ore gap energy to the upper limit of the Ore gap. The problems with this model are the uncertainty of the choice of the upper energy limit and the decrease in P, due to positrons being removed from the Ore gap by inelastic or

capture processes.

More recently, Mogensen[4] relates positronium formation to the reactions between positrons and electrons in the positron spur. The positron spur is the group of reactive intermediates (the positron, electons, positive ions, etc.) which are created when the positron loses the last amount of its kinetic energy. Here positronium formation must compete with electron-ion recombination and electron and positron reactions with molecules of the medium. This model is termed the spur reaction model. The positronium yield in this model is a function of the yield of the various constituents of the spur and the various reaction and recombination rates in competition with each other. At this stage in its development, the theory has been moderately successful in qualitative predictions of positronium yields.

A positron in a Ps atom may annihilate either with its own electron or with an electron from the surrounding medium. In the case of o-Ps, the observed annihilation rate in condensed materials is substantially greater than the vacuum rate of 1/140 $nsec^{-1}$. This is generally accepted to be due to pickoff annihilation of the Ps positron with an electron of the surrounding medium, where the positron and this electron are in a singlet spin configuration at the time of annihilation. Positrons in p-Ps, will also be subject to pickoff annihilation, but to a lesser extent due to the relatively

short natural lifetime of this state (i.e. most p-Ps positrons will annihilate with their own electron). Numerous attempts have been made to explain this pickoff rate of o-Ps which has been found to depend on many different properties of the medium such as electron polarizeability[5], temperature[6], density[7], and surface tension[6]. Brandt et al.[8] developed a theory which correlated the pickoff rate to the amount of "free volume" available in a substance. By "free volume" is meant the region within the medium not actually occupied by the molecules of the medium. Bisi et al.[7], on the other hand, followed a semi-empirical approach which assigned an effective number of electrons for pickoff to each atom of the molecule of the medium. Using this effective number of electrons and an equation of the same form as (1.1), they were able to predict the pickoff rates of o-Ps in different substances with reasonable accuracy. Recently, Buchikhin et al.[9] have employed a theory similar to the free volume theory for organic liquids in which the "free volume" is replaced by a cavity in the material created by the balance of various molecular forces inside the liquid with the zero point pressure of the positronium atom. In this model the annihilation rate depends on the extent to which the Ps atom penetrates through the walls of the cavity into the surrounding medium. In the present investigation, this type of approach is termed the "bubble" model and an extensive expansion of this is contained in Chapter 2.

1.6 Experimental Methods

Several experimental methods are available for the study of positron annihilation. The most common method is the lifetime method where the mean lifetime of positrons from ^{22}Na is measured with respect to a 1.28 Mev gamma ray which is emitted simultaneously with the positron. Typical source strengths used are approximately 10 μCi. Instrumental resolutions of the order of 300 psec are easily achieved with presently available instrumentation. Computer programs are now available which are able to separate several lifetime components in the composite lifetime spectra. This method yields a series of lifetimes (or annihilation rates) and intensities corresponding to different modes of annihilation.

Another method is that of angular correlation. In this method, the angular distribution of the two-gamma coincidence rate is measured. The resulting count rate curve may readily be converted to a momentum distribution of the annihilating positron-electron pairs. Normally, in such a momentum distribution, a low momentum component and a high momentum component are easily identifiable. The low momentum component corresponds to the self annihilation of nearly thermalized p-Ps, while the high momentum component results from the annihilation of positrons with electrons from the surrounding medium. The strength of the positron source in this case must be greater (by at least two orders of magnitude) than in the case of the lifetime experiment.

The rare three-gamma annihilation of the triplet state of Ps may be observed directly in a triple coincidence experiment or by examining the change in the gamma-ray spectrum due to the additional continuous energy distribution of gammas from three-gamma events.

The most recently developed method for the study of positron annihilation is the Doppler broadening technique which yields the same information as the angular correlation technique. This method uses a Ge(Li) detector with very high resolution to measure the Doppler broadening of the 0.511 MeV annihilation radiation due to the momentum of the annihilating positron-electron pair. The count rate distribution in this case can be treated in a similar manner to that of the angular correlation count rate curve. There is one difference however, in that the instrumental broadening in this case is significantly greater than the broadening due to finite slit width in the angular correlation case. This problem has recently been solved with the development of computer programs to deconvolute the experimental spectrum and produce the "true spectrum", devoid of instrumental effects.[10] Due to this latest development, the Doppler broadening technique offers decided advantages over the angular correlation method. Whereas the angular correlation data acquisition time is of the order of the days, the Doppler broadening data acquisition time is typically 200 minutes. The source used may be as as small as a few μCi as opposed to several mCi in the

angular correlation case and the possibility of secondary effects such as radiation damage or other radiation induced effects is greatly reduced.

Chapter II

THE THEORY OF THE BUBBLE MODEL

2.1 Introduction

The assumption of complete thermalization of positronium in a liquid leads to a contradiction as a result of the uncertainty principle since, in a liquid, the positronium must have a localized state. That is to say, a non-localized or Bloch state such as might occur in a periodic crystal structure is not possible here. From the Heisenberg uncertainty principle,

$$(2.1) \qquad \Delta x \, \Delta p \geq \hbar ,$$

it can be seen that a free particle with a zero point momentum p_z cannot be localized to a greater degree than $\hbar/p_z$. If the zero point energy of the positronium atom were taken to be the thermal energy of the medium containing the positronium, i.e. if $E_z \sim kT$, then $p_z = \sqrt{2mE_z} \sim \sqrt{2mkT}$ and

$$(2.2) \qquad \Delta x \geq \hbar/\sqrt{2mkT} .$$

If T is taken to be $300^{\circ}K$ and m twice the rest mass of the electron, then this results in $\Delta x \geq 8.6\text{Å}$. Thus the positronium cannot be contained within a sphere of radius less than $R=8.6\text{Å}$. But distances between molecules in a liquid such as hexane are of the order of 1Å, much less than the required distance of 17.2Å. Thus, the assumption of thermalization in a free state (without further interaction with the surroundings) leads to a rather serious contradiction.

In the above picture, it becomes clear that the zero point motion of the positronium atom will exert outward pressure on the molecules of the medium, forcing the formation of a small bubble. Hence, the term "bubble model" is commonly used for this description. This repulsive force is in equilibrium with the inward pressure of the surface of the bubble which is a function of the surface tension and pressure exerted on the medium. Thus, the radius, R, of the bubble will be less than the Δx calculated above and the bound state zero-point energy will be greater than kT. A quantum mechanical treatment of the bubble model should verify the preceding conclusions.

This approach was first suggested by Ferrel[11] to apply to positronium in liquid helium, where the model was later termed the bubble model. Roellig[12] and Briscoe et al.[19] have made extensive use of this model as applied to liquid helium. Later, Buchikhin et al.[9] and Tao[6] have applied this model to molecular liquids in general.

2.2 Quantum Mechanical Treatment

This problem can be simply described since there is spherical symmetry. The positronium atom exists within a bubble containing no molecules of the surrounding medium.[12] Inside the bubble the potential will be zero, and outside it will be constant. The potential outside the bubble, V_o, is the barrier height against adiabatic penetration of the positronium atom into the medium from a vacuum.[13] Thus, assuming that the bubble has a very sharply defined surface, a good model will be a spherical potential well of depth V_o and radius R with an infinitely steep side.

Several important further assumptions will be made in the treatment of the potential problem and for convenience they are listed below.

(1) The positronium wave function is separable into the product of a wave function $\Psi_{cm}(\bar{r}_o)$ for the centre of mass coordinate $\bar{r}_o = (\bar{r}_+ + \bar{r}_-)/2$, and a wave function $\Psi_{ep}(\bar{r})$ for the electron-positron relative coordinate, $\bar{r} = \bar{r}_+ - \bar{r}_-$, where $\bar{r}_+$ and $\bar{r}_-$ are the coordinates of the positron and electron, respectively.

(2) Since it has been shown that if the wave function $\Psi_{ep}(\bar{r})$ is ignored, no great error will be introduced into the calculation,[13] only Ψ_{cm} will be considered. Thus, $\Psi_{cm}(\bar{r}_o)$ is renamed $\Psi(\bar{r})$ and taken to be the total wave function.

(3) The potential well is shallow enough so that the corresponding Schrödinger equation for the centre of mass wave

function yields only s states as allowed bound state solutions.

It should be noted that the disregarding of the inter-atomic wave function also means disregarding the spin-orbit coupling term in the Hamiltonian of the associated Schrödinger equation, as the coupling term is a function of the inter-atomic coordinate[14].

The Schrödinger wave equation may now be applied in the following form:

$$(2.3) \qquad \left(\frac{\hbar^2}{2M}\nabla^2+V-E\right)\Psi(r,\theta,\phi) = 0$$

It is assumed, as usual, that the centre of mass wave function is separable into an angular and a radial part, i.e.,

$$(2.4) \qquad \Psi(r,\theta,\phi) = \psi(r)\ Y_\ell^m(\theta,\phi)$$

The angular part $Y_\ell^m(\theta,\phi)$ consists of the spherical harmonics, resulting from the use of spherical polar coordinates. The potential is spherically symmetric and may be written as

$$(2.5) \qquad V = O \qquad O \leq r \leq R$$

$$(2.6) \qquad V = V_o \qquad r \geq R$$

If the Laplacian ∇^2 is written in spherical polar coordinates, the Schrödinger equation will be separable. In spherical polar coordinates,

$$(2.7) \qquad \nabla^2 \equiv \frac{1}{r}\frac{\partial^2}{\partial r^2}(r)+\frac{1}{r^2\sin\theta}\frac{\partial}{\partial\theta}\left\{\sin\theta\frac{\partial}{\partial\theta}\right\}+\frac{1}{r^2\sin^2\theta}\frac{\partial^2}{\partial\phi^2}$$

With some rearranging and dividing by $\Psi(r)Y_\ell^m(\theta,\phi)$, the Schrödinger equation may be rewritten

$$(2.8) \qquad \frac{\hbar^2 r}{2M\psi(r)}\frac{\partial^2}{\partial r^2}\{r\psi(r)\}+r^2\{E-V(r)\}$$
$$+\frac{1}{Y_\ell^m(\theta,\phi)\sin\theta}\frac{\partial}{\partial\theta}\left\{\sin\theta\frac{\partial}{\partial\theta}Y_\ell^m(\theta,\phi)\right\}$$
$$+\frac{1}{Y_\ell^m(\theta,\phi)\sin^2\theta}\frac{\partial^2}{\partial\phi^2}Y_\ell^m(\theta,\phi) = O.$$

Note that V has been written as V(r) since the potential is only dependent on the radial distance r from the origin. The Schrödinger equation has been separated into two independent parts. Since the sum of the two independent terms is zero, each must be equal to zero, or at most a constant, usually written in the form $\ell(\ell + 1)$. The separated radial equation for $0 \leq r \leq R$ is

$$(2.9) \quad \frac{d^2}{dr^2}\{r\psi(r)\}+\{\frac{4m_e}{\hbar^2}E-\frac{\ell(\ell+1)}{r^2}\}r\psi(r) = 0$$

Here $2m_e$ has been substituted for M since the mass M of the positronium atom is twice the mass of the electron. If a change of variables to $\rho = (4m_eE/\hbar^2)^{\frac{1}{2}}r$ is made in the above equation it can be written in the form of Bessel's equation, of which the solutions are spherical Bessel functions[15]. However, for the singlet state of the well the orbital angular momentum is equal to zero. Thus $\ell = 0$ in the above radial equation. It now becomes

$$(2.10) \quad \frac{d^2}{dr^2}\{r\psi(r)\}+ k_1^2 r\psi(r) = 0$$

where $k_1^2 = \frac{4m_e}{\hbar^2}E$

The only solution $\psi(r)$ which does not diverge at r = 0 is

$$(2.11) \quad \psi(r) = \frac{A\sin(k_1 r)}{r} \qquad 0 \leq r \leq R$$

Similarly, if

$$(2.12) \quad k_2^2 = \frac{4m_e(V_0 - E)}{\hbar^2}$$

the radial equation for $r \geq R$ becomes

$$(2.13) \quad \frac{d^2}{dr^2}\{r\psi(r)\} - k_2^2 r\psi(r) = 0$$

The only solution which does not diverge when $r \to \infty$ is

$$(2.14)\quad \psi(r) = \frac{B\exp(-k_2 r)}{r} \qquad r \geq R$$

The angular equation will be

$$(2.15)\quad \frac{1}{Y_\ell^m(\theta,\phi)\sin\theta}\frac{\partial}{\partial\theta}\left\{\sin\theta\frac{\partial}{\partial\theta}Y_\ell^m(\theta,\phi)\right\} + \frac{1}{Y_\ell^m(\theta,\phi)\sin^2\theta}\frac{\partial^2}{\partial\phi^2}Y_\ell^m(\theta,\phi)+\ell(\ell+1) = 0.$$

The acceptable solutions to this equation are the spherical harmonics

$$(2.16)\quad Y_\ell^m(\theta,\phi) = P_\ell^m(\cos\theta)\exp(im\phi)$$

where $P_\ell^m(\cos\theta)$ are the associated Legendre polnomials. Since $\ell = 0$ and thus $m = 0$ from the restriction $|m| \leq \ell$ the only spherical harmonic needed is[16]

$$(2.17)\quad Y_o^o(\theta,\phi) = \frac{1}{\sqrt{4\pi}} .$$

Boundary conditions for the radial wave functions are that the wave function and its slope must be continuous at $r = R$. This results in two boundary conditions,

$$(2.18)\quad A\sin(k_1 R) = B\exp(-k_2 R) \quad \text{and}$$

$$(2.19)\quad Ak_1 R\cos(k_1 R) - A\sin(k_1 R) = -Bk_2 R\exp(-k_2 R) - B\exp(-k_2 R)$$

which are referred to as the first and second boundary condition, respectively. Two ratios A/B may be derived: one from the first boundary condition and one from the sum of the two boundary conditions. If the two ratios A/B are equated, the following secular equation results:

$$(2.20)\quad k_1 R\cot(k_1 R) = -k_2 R.$$

Another convenient form of this equation may be arrived at if it is squared, a trigonometric identity is applied and then only the positive root is retained, resulting in

$$(2.21)\quad \frac{k_1 R}{\sin(k_1 R)} = \left(\frac{4m_e V_0}{\hbar^2}\right)^{\frac{1}{2}} R.$$

This can also be rewritten as

$$(2.22)\quad E = V_0 \sin^2\left(\left\{\frac{4m_e E}{\hbar^2}\right\}^{\frac{1}{2}} R\right).$$

The most convenient form of the above secular equations may be employed to solve (graphically) for the energy of the bound state.

In order to determine the normalization constants A and B the total wave function must be normalized. The normalization equation is

$$(2.23)\quad \int_0^\infty \Psi\Psi^* d^3r = A^2 \int_0^R \int_0^{2\pi} \int_0^\pi Y_\ell^m(\theta,\phi) Y_\ell^{m*}(\theta,\phi) \sin\theta d\theta d\phi \cdot \frac{\sin^2(k_1 R)}{r^2} r^2 dr$$
$$+A^2 \int_R^\infty \int_0^{2\pi} \int_0^\pi Y_\ell^m(\theta,\phi) Y_\ell^{m*}(\theta,\phi) \sin\theta d\theta d\phi \frac{\sin^2(k_1 R)}{\exp(-2k_2 R)} \cdot \frac{\exp(-2k_2 r)}{r^2} r^2 dr$$

Part of the above integral may be simplified as follows due to the orthogonality of the Y_ℓ^m :

$$(2.24)\quad \int_o^{2\pi} \int_o^\pi \frac{\sin\theta d\theta d\phi}{4\pi} = \int_o^{2\pi} \frac{d\phi}{2\pi} = 1$$

The fact was used that $Y_\ell^m = Y_o^o = \frac{1}{\sqrt{4\pi}}$ for the singlet state. The normalization equation then simplifies to

$$(2.25)\quad A^2 \int_o^R \sin^2(k_1 R) dr + A^2 \int_R^\infty \frac{\sin^2(k_1 R)}{\exp(-2k_2 R)} \exp(-2k_2 r) dr = 1.$$

After considerable manipulation this yields

$$(2.26)\quad A^2 = \frac{2k_1 \cot(k_1 R)}{k_1 R \cot(k_1 R) - 1}$$

The foregoing relations then summarize the quantum mechanical treatment in the position representation.

The wave function in the momentum representation, however, is also needed in order that one may determine the distribution of positronium in momentum space. The wave function in the momentum representation is just the Fourier transform of the position representation wave function, or

$$(2.27)\quad \Psi(\bar{k}) = \frac{1}{(2\pi)^{3/2}} \int d^3r \exp(-i\bar{k}\cdot\bar{r})\ \Psi(r) Y_{\ell}^{m}(\theta,\phi).$$

The fact that $\ell = m = 0$ in the singlet state is neglected for the moment. One sets $\Psi(\bar{r}) = \Psi(r)$ due to the spherical symmetry. The notation $\bar{k}$ used for momentum will be understood to be in units of length^{-1}. This is merely the ordinary momentum $\bar{p}$ divided by $\hbar$.

The exponential $\exp(-i\,\bar{k}\cdot\bar{r})$ may be expanded into spherical harmonics Y_{ℓ}^{m} of the angle γ between the vectors $\bar{r}$ in the direction θ,ϕ and $\bar{k}$ in the direction Θ,Φ [17] so that

$$(2.28)\quad \exp(-i\bar{k}\cdot\bar{r}) = \sum_{\lambda=0}^{\infty} \sqrt{4\pi(2\lambda+1)}\, i^{-\lambda} j_{\lambda}(kr) Y_{\lambda}^{o*}(\cos\gamma)$$

where $j_{\lambda}(kr)$ is the spherical Bessel function of order λ. Here $Y_{\lambda}^{o}(\cos\gamma)$ may be expressed by the polar angles of $\bar{r}$ and $\bar{k}$ using the addition theorem of spherical harmonics,

$$(2.29)\quad Y_{\lambda}^{o}(\cos\gamma) = \sqrt{\frac{4\pi}{2\lambda+1}} \sum_{\mu=-\lambda}^{+\lambda} Y_{\lambda}^{\mu *}(\Theta,\Phi) Y_{\lambda}^{\mu}(\theta,\phi).$$

Combining these relations with the Fourier transform one gets:

$$(2.30)\quad \Psi(\bar{k}) = \frac{4\pi}{(2\pi)^{3/2}} \int_0^{\infty} r^2 dr \int_0^{2\pi} \int_0^{\pi} \sin\theta\, d\theta\, d\phi$$

$$\cdot \sum_{\lambda\mu} i^{-\lambda} j_{\lambda}(kr) Y_{\lambda}^{\mu}(\Theta,\Phi) Y_{\lambda}^{*}(\theta,\phi) Y_{\ell}^{m}(\theta,\phi) \Psi(r).$$

But

$$(2.31)\quad \int_0^{2\pi}\int_0^{\pi} \sin\theta\, d\theta\, d\phi\, Y_\lambda^{\mu *}(\theta,\phi) Y_\ell^m(\theta,\phi) = \delta_{\ell\lambda}\delta_{m\mu}$$

so that only the ℓ, m term remains of the double sum above and results in

$$(2.32)\quad \psi(\bar{k}) = \frac{4\pi}{(2\pi)^{3/2}(4\pi)^{1/2}} \int_0^{\infty} r^2 dr\, j_0(kr)\, \Psi(r)$$

after setting $\ell = m = 0$. But the spherical Bessel function of zero order is

$$(2.33)\quad j_0(kr) = \sin(kr)/kr.$$

Substituting the actual wave functions into the transformation equation one gets

$$(2.34)\quad \Psi(\bar{k}) = \frac{1}{\sqrt{2\pi}} \frac{A}{k} \left(\int_0^R dr\, \sin(k_1 r)\, \sin(kr) + \int_R^{\infty} dr\, \sin(k_1 R)\, \exp(k_2 R)\, \sin(kr) \exp(-k_2 r) \right)$$

The first integral is solved as follows from standard integration tables:

$$(2.35)\quad \int_0^R dr\, \sin(k_1 r)\, \sin(kr) = \frac{\sin(k_1 R - kR)}{2(k_1 - k)} - \frac{\sin(k_1 R + kR)}{2(k_1 + k)}$$

The second integral is solved with a change of limits (setting $r = x + R$) as follows

$$(2.36)\quad \int_R^{\infty} dr\, \sin(k_1 R) \exp(k_2 R) \sin(kr) \exp(-k_2 r)$$
$$= \int_0^{\infty} dx\, \sin(k_1 R) \sin\{k(x+R)\} \exp(-k_2 x)$$
$$= \frac{\sin(k_1 R)}{k_2^2 + k^2} \left(k\cos(kR) + k_2 \sin(kR) \right).$$

Thus

$$(2.37)\quad \Psi(\bar{k}) = \frac{1}{\sqrt{2\pi}} \frac{A}{k} \left(\frac{\sin(k_1 R - kR)}{2(k_1 - k)} - \frac{\sin(k_1 R + kR)}{2(k_1 + k)} \right.$$

$$+ \frac{\sin(k_1 R)}{k_2^2 + k^2}\{k\cos(kR) + k_2\sin(kR)\}\Bigg]$$

This expression can be simplified considerably if all factors are brought under a common denominator, the trigonometric terms with sums and differences as arguments are expanded with trigonometric identities, and use is made of the first secular equation written above for the potential well and repeated here for convenience sake:

$$(2.20)\quad k_1 R\cot(k_1 R) = -k_2 r$$

Then after considerable manipulation one arrives at

$$(2.38)\quad \Psi(\bar{k}) = \frac{1}{\pi}\frac{R^{3/2}}{kR}\left[\frac{k_1 R\cot(k_1 R)}{k_1 R\cot(k_1 R) - 1}\right]\cdot\left[\frac{(k_1 R)^2 + (k_2 R)^2}{(k_1 R)^2 - (kR)^2}\right]$$

$$\cdot\left[\frac{kR\sin(k_1 R)\cos(kR) - k_1 R\cos(k_1 R)\sin(kR)}{(k_2 R)^2 + (kR)^2}\right]$$

This wave function obeys the normalization condition

$$(2.39)\quad \int_0^{\infty}\int_0^{2\pi}\int_0^{\pi} k^2\, dk\, d\theta\, d\Phi\, |\Psi(\bar{k})\ Y_{\ell}^{m}(\theta,\Phi)|^2 = 1.$$

The above normalization equation was integrated numerically by computer with the condition $\ell = m = 0$ for the singlet state, and shown to hold true. Equation (2.38) may be modified to the same form as the result presented by Buchikhin *et al*[9]. Note however that their result is incorrect, probably due to misprints.

2.3 Application to Doppler Spectra

Consider a positron-electron pair with momentum $\bar{p}$ which annihilates and produces two gamma-rays, one of which is detected by a Ge(Li) detector. The direction from the positron-electron pair to the detector will be labelled x. To first order, this is the only component of the positron-electron momentum affecting the Doppler energy shift of the 511 KeV gamma rays emitted. This is true since the deviation from 180^{o} between the two emitted gamma-rays is typically less than 10 milliradians (see figure 2.1). Then conservation of energy and momentum for the photons given off in opposite directions require that

$$(2.40) \quad 2m_e c^2 = h\nu + h\nu' \text{ and}$$

$$(2.41) \quad P_x = h\nu/c - h\nu'/c$$

where m_e is the rest mass of the electron, c the speed of light and $h\nu$ and $h\nu'$ the two photon energies. However, if the energy $m_e c^2$ is rewritten as $h\nu_o$ or the photon energy when the positron-electron momentum is zero, then upon combining the above 2 relations, the result is

$$(2.42) \quad P_x = 2(h\nu - h\nu_o)/c \quad \text{or}$$

$$P_x = 2\Delta E/c$$

which relates the Doppler shift in photon energy, ΔE, to the electron-positron pair momentum component, P_x. Or, changing to momentum units of length^{-1},

(2.43) $k_x = 2\Delta E/hc.$

One assumes that the gamma-ray spectrum from the annihilating pair is accumulated in a multi-channel analyser. The total number of counts at a particular energy E, C(E) is then proportional to the total number of annihilating pairs whose x-component of momentum is k_x. The total number of such pairs is obtained by integrating the momentum space density $\rho(k)$ over a plane of constant k_x (see figure 2.2). Thus

(2.44) $C(E) = \text{const} \times \int\int \rho(k)\,dk_y dk_z.$

By assuming the distribution in momentum space to be isotropic (a valid assumption in a liquid), the integral becomes

(2.45) $C(E) = \text{const} \times 2\pi \int_{k_x}^{\infty} k\rho(k)\,dk$

where the limit k_x arises from the fact that at $k_y=k_z=0$, $k=k_x$ since $k^2= k_x^2+ k_y^2+ k_z^2$. The general rule for differentiating (with respect to k_x) under the integral sign yields

(2.46) $\rho(k_x)= \frac{-1}{\text{const} \times 2\pi} \frac{1}{k_x} \frac{dC(e)}{dk_x}$.

Since, by definition, $\rho(k_x)$ is the momentum space density of electron-positron pairs with the value of the total momentum equal to k_x, the subscripts above may be dropped and the relation becomes

(2.47) $\rho(k) = \frac{-1}{\text{const} \times 2\pi} \frac{1}{k} \frac{dC(E)}{dk}$

Thus, it can be seen that the derivative of the counting rate curve is simply related to the momentum space density function, $\rho(k)$. Furthermore, due to the spherical symmetry, the momentum distribution is given by [18]

(2.48) $N(k) = 4\pi k^2\, \rho(k)$

The momentum space density function may also be calculated from the square of the positronium wave function in the momentum representation. Then,

$$(2.49) \quad N(k) = 4\pi k^2 \, | \psi (\bar{k}) |^2 ,$$

where $\psi(\bar{k})$ for the bubble model is given by equation (2.38).

The narrow part of the counting rate distribution of the Doppler spectrum (assuming no instrumental broadening) is due to the annihilation of p-Ps. This part may be described by a Gaussian,

$$(2.50) \quad C(E) = \frac{A}{\sqrt{\pi}\,\sigma} \exp(-\Delta E^2/\sigma^2)$$

where the full width at half maximum of the curve, Γ is related to σ by,

$$(2.51) \quad \Gamma = 2(\ell n 2)^{\frac{1}{2}}\, \sigma .$$

If ΔE and σ are written in terms of momentum, k, and the photon momentum is related to the electron-positron momentum k, then the momentum distribution may be written as

$$(2.52) \quad N(k) = \frac{4A}{\sqrt{\pi}} \frac{k^2}{\sigma^3} \exp(-k^2/\sigma^2) .$$

N(k) is properly normalized so that

$$(2.53) \quad \int_0^\infty N(k) = A.$$

Thus, if σ in momentum units is known for the narrow component of the Doppler peak, then the experimental momentum distribution may be calculated. Expressions (2.49) and (2.52) may be compared and the parameters $k_1 R$ and R arising from $\psi(\bar{k})$ in (2.49) may be adjusted in a least square fashion to fit expression (2.49) to (2.52).

Figure 2.1

Illustration of Momentum Conservation upon Positron-electron Pair Annihilation

Figure 2.2

Illustration of Two Ways to Integrate the Momentum Density over a Plane in Momentum Space

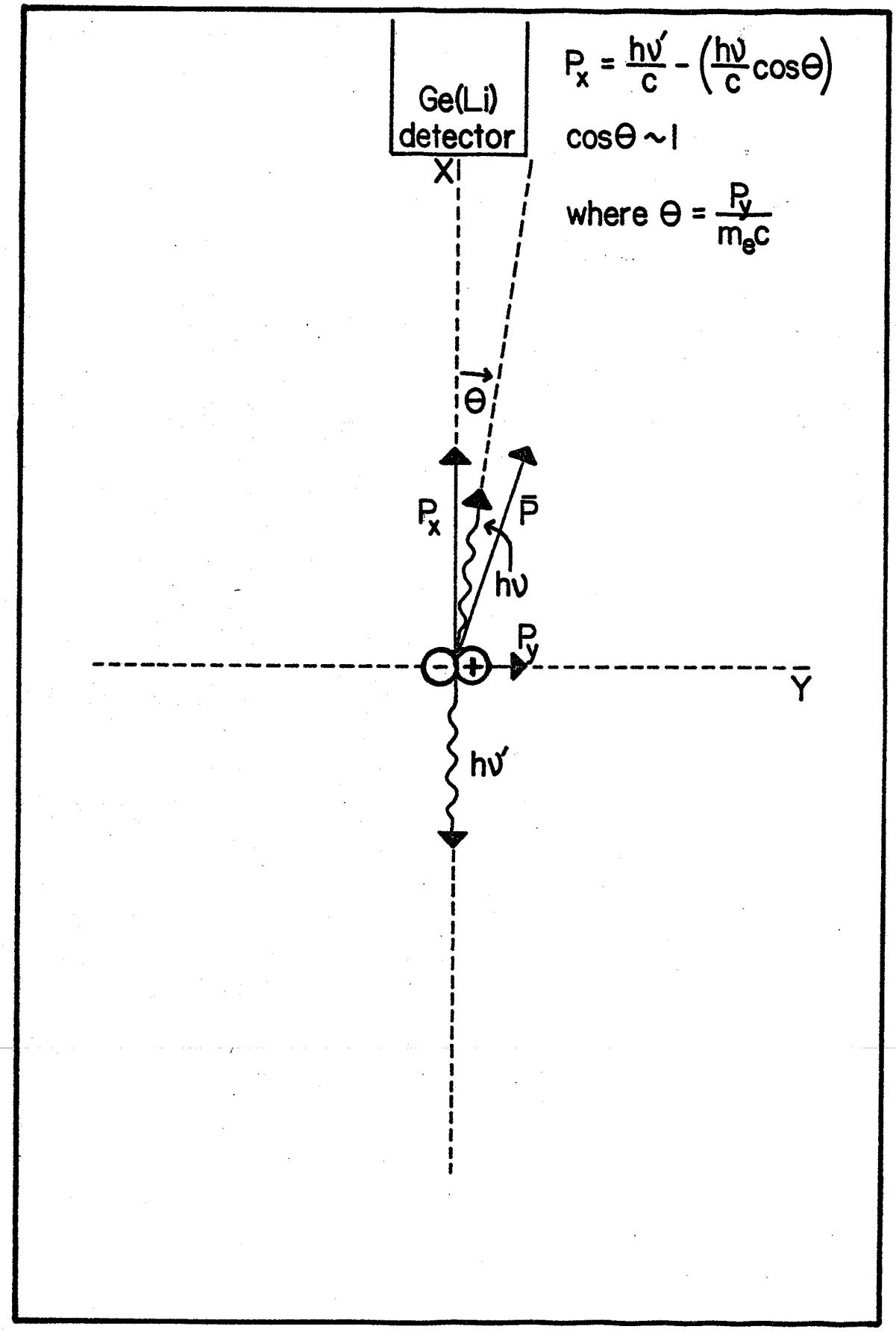
Ge(Li)
detector
X
$P_x = \frac{h\nu'}{c} - \left(\frac{h\nu}{c}\cos\Theta\right)$
$\cos\Theta \sim 1$
where $\Theta = \frac{P_y}{m_e c}$
$\vec{\Theta}$
P_x
$\vec{P}$
$h\nu$
P_y
Y
$h\nu'$

$$\int_{-\infty}^{\infty}\int_{-\infty}^{\infty} dk_y\, dk_z\, \rho(\vec{k})$$

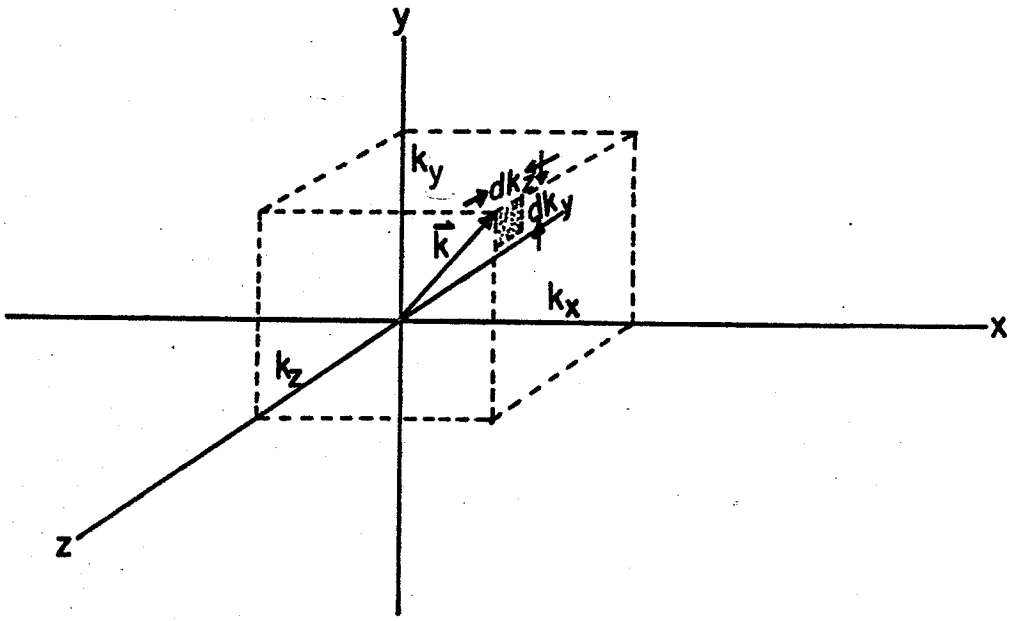

$$2\pi \int_{k_x}^{\infty} k\, dk\, \rho(k)$$

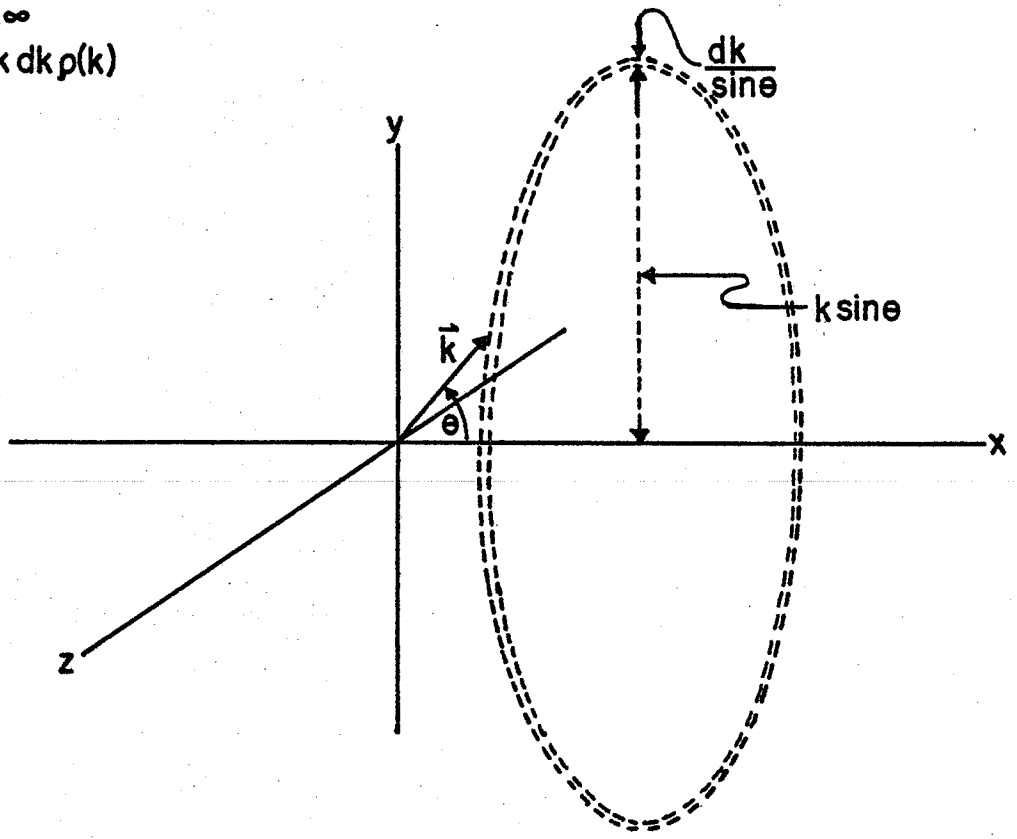

2.4 Application to Lifetime Spectra

In most organic liquids, one observes a long lifetime component, of lifetime greater than 1 nsec but less than 5 nsec[s]. This component is attributed to the annihilation of o-Ps but is much shorter than the vacuum lifetime of o-Ps of 140 nsec. As described earlier the process shortening this lifetime is termed "electron pickoff" and is due to the fast para annihilation of the positron from the o-Ps with an electron from a molecule of the surrounding medium.

Employing a development similar to that of Brandt *et al*[8] in the free volume model the pickoff rate may be expressed as

$$(2.54) \quad \lambda_p = \pi r_o^2 \, c\rho_o \int_{v_o} \psi_{ps} \, \psi_{ps}^* \, d^3r$$

where r_o is the classical electron radius, c the velocity of light, ρ_o the effective number of electrons per unit volume and v_o the "excluded volume", in this case the volume outside of a sphere of radius R. The assumptions made in writing the above relation are:

(1) The mutual positronium-molecule polarization may be neglected.

(2) The inter-atomic portion of the positronium wave function may be neglected.

(3) The positronium in the liquid "sees" a finite spherical potential well with infinitely steep sides.

Using the singlet positronium wave function previously developed yields

$$(2.55)\quad \int_{V_o} \Psi_{ps}\,\Psi_{ps}^{*}\,d^3r = \frac{2k_1\cot(k_1R)}{k_1R\cot(k_1R)-1}\,\frac{\sin^2(k_1R)}{\exp(-2k_2R)} \cdot \int_R^{\infty} \exp(-2k_2r)\,dr = \frac{\sin^2(k_1R)}{1-k_1R\cot(k_1R)}$$

The pickoff rate, however, cannot be directly equated to the observed annihilation rate. The positronium annihilates with both the vacuum rate λ_{vac} and λ_p. Then the observed annihilation rate must be written as

$$(2.56)\quad \lambda_{obs} = \lambda_{vac} + \lambda_p$$

and upon combining (2.54), (2.55) and (2.56),

$$(2.57)\quad \lambda_{obs} - \lambda_{vac} = \pi r_o^2 c\rho_o \left[\frac{\sin^2(k_1R)}{1 - k_1R\cot(k_1R)}\right] .$$

It should be noted that the λ_p used here is the "actual pickoff rate" and not the "pickoff rate if the positronium were totally in the medium", as formulated by Roellig[12]. Equation (2.57) then provides another means of calculating the well parameter k_1R.

2.5 The Bubble Model and Surface Tension

The bubble size may be related to the surface tension by minimizing the Gibbs' free energy of the system with respect to the radius R:[19]

$$(2.58)\quad G = 4\pi(R-Z_0)^2\gamma + P\pi\frac{4}{3}R^3 + E_z + G_{sp} + G_{BT}\ .$$

Here R is the radius of the bubble, γ the surface tension, P the pressure, E_z the zero point energy of the positronium, and G_{sp} and G_{BT} contributions from surface phonons and translational motion of the whole bubble. The factor Z_0 is a correction to the energy term introduced due to the inadequacy of this thermodynamic treatment for very small bubbles. Tolman[20] states that as one considers smaller and smaller droplets of liquid phase, the previously satisfactory thermodynamic methods and concepts of surface tension seem less and less appropriate. Only the first and third term on the right hand side of equation (2.58) will be considered. It has been found in this work that neglecting the pressure term for a pressure equal to the vapour pressure of a liquid typically introduces an error of less than .01%. Surface vibrations and translational motion are assumed negligible. Upon differentiating equation (2.58) one gets,

$$(2.59)\quad \frac{dE_z}{dR} + 8\pi\ (R - Z_0)\gamma = 0.$$

The secular equation (2.22) is combined with equation (2.59). After some manipulation, differentiation of equation (2.22) yields

$$(2.60)\quad \frac{dE_z}{dR} = \frac{2k_1E}{\tan\ (k_1R) - k_1R}.$$

In combination with equations (2.21) and (2.22) this leads to the relation

$$(2.61)\quad \frac{\sin^4(k_1R)}{k_1R(k_1R - \tan k_1R)} = \frac{\pi h^2\gamma}{m_e V_0^2}\left(1 - \frac{Z_0}{R}\right).$$

Alternatively (2.21) may be used to eliminate V_0 from (2.61) to give the relation

$$(2.62)\quad R^4 = \frac{h^2}{16\pi m_e}\cdot\frac{k_1R}{k_1R - \tan(k_1R)}\cdot\frac{1}{\{1 - \frac{Z_0}{R}\}\gamma}.$$

The value of the parameter Z_0 is difficult to determine and is usually set equal to zero. Then, if the values of k_1R and γ are known for a particular sample, the well depth V_0 may be calculated from (2.61) and the radius of the bubble may be calculated from (2.62).

Equations (2.61) and (2.62) can be solved exactly if experimental values of k_1R are known - this will be done in a succeeding section. It is instructive, however, at this point, to examine limiting cases in a direct fashion. For example $\gamma = 18.1$ dynes/cm for hexane at room temperature and with $Z_0 = 0$ one may establish limiting values for E_z, V_0 and R. For the first limiting case one lets $E_z = V_0$ and assumes that only one bound state is possible. This will give the absolute minimum value of E_z and V_0 and the corresponding value of R for a typical value of surface tension. From the secular equation (2.20)

$$(2.63)\quad k_1R\cot(k_1R) = 0 \quad \text{or} \quad \cos\left\{\frac{4m_eE_z}{h}\right\}^{\frac{1}{2}}R = 0.$$

Thus

$$(2.64)\quad E_z = \frac{\pi^2h^2}{16m_eR^2}$$

for case 1. Substitution of this E_z into equation (2.59)

and setting $Z_0 = 0$ yields R = 4.27Å. This case corresponds to an energy $E_z = 0.26$ eV. In the second limiting case two bound states are allowed, the upper one having energy $E_z = V_0$. This value is also equal to the upper limit for E_z and V_0 for the case with one bound state. Again from equation (2.20)

$$(2.65) \quad E_z = \frac{9\pi^2 h^2}{16 m_e R^2}$$

for case 2. Substitution of this E_z into equation (2.59) yields R = 7.39 Å. This corresponds to an energy $E_z = 0.77$ eV. Thus $0.26 \leq E_z \leq 0.77$. It should be noted that the minimum energy predicted is a factor of ten greater than thermal energy (kT) at room temperature.

Chapter III

EXPERIMENTAL METHODS

3.1 The Doppler Experiment

With the development of high resolution Ge(Li) detectors, low noise amplifiers and digital gain stabilizers, the measurement of the Doppler broadened electron-positron annihilation spectrum (i.e. C(E) in equation 2.47) has become feasible. In this investigation, an Ortec model 450 research amplifier, together with a digitally-stabilized Kicksort 512 channel multichannel analyser and an Ortec model 8101-1020V Ge(Li) detector, proved to be a satisfactory system (see figure 3.1).

The Ge(Li) detector head was shielded on the sides, front, bottom and top, with from 2 to 4 inches of lead. All lead bricks used were carefully checked for any ^{22}Na contamination before being used. Radioactive sources not actually in use were removed from the vicinity of the detector and well shielded. With these precautions, the ^{22}Na peak with no source present within the lead shield was kept at a level below 50 counts above background in a 200-minute accumulation period. This represented less than .01% of the typical experimental peak height accumulated in 200 minutes or only 7% of one standard deviation in the peak of an experimental spectrum.

The gain of the system was adjusted by varying the gain of the amplifier and the rundown rate (digital gain) of the multichannel analyser. Varying the rundown rate and zero of the multichannel analyser eliminated the necessity of

using a biased amplifier in the system in order to expand the width of the peak in the spectrum. The digital stabilizer was used only for gain correction. Gain stabilization is achieved as follows. A reference peak, which in this case is always the actual peak of interest in the experiment, is divided into two regions of variable width, located symmetrically about the centre of the peak. The gain stabilizer, which has a variable sensitivity, adjusts the gain positively if a count falls into the lower region and negatively if a count falls into the upper region. Therefore, the gain is adjusted if there is a real gain shift in the system but also responds to statistical variations in the numbers of counts falling into the two regions. Even if the system gain is constant, this always results in a small increase of the width of the experimental peak. Therefore, considerable care must be used in employing gain stabilization in order to avoid undue widening of the peak. It is necessary to compromise between the artificial peak widening due to statistics and rapid gain correction which is desirable in the case of a real gain shift.

The system energy resolution was determined using the 0.514 MeV gamma ray of ^{85}Sr. With the use of both the 0.511 ^{22}Na and 0.514 MeV ^{85}Sr gamma rays, the system energy calibration may be determined. Two precautions must be taken when setting the system gain and determining the calibration factor. First, due to the digital nature of the gain correct-

ion, the gain of the system may only be set at a value which initially registers a zero correction for both the 0.511 and 0.514 MeV sources run for a short period rapidly in succession. (It is assumed that there will be no gain shift between two such spectra.) Second, the system gain and resolution is dependent on the total count rate. The count rate was, therefore, held constant at 4.3 kHz for all experimental accumulations. This rate was considered to be a reasonable compromise between better counting statistics and worse resolution. The system energy calibration so determined was held constant at 0.1154 KeV/channel. Based upon the assumption that the ^{85}Sr 0.514 MeV gamma spectrum well approximates the energy resolution at 0.511 MeV, the 0.514 spectrum was used directly as the system resolution function. A typical resolution spectrum of ^{85}Sr with a FWHM of 1.53±.05 KeV is displayed in figure 3.3.

Several Doppler broadened spectra were accumulated overnight for each sample (with the multichannel analyser set at automatic mode). A resolution spectrum was also accumulated each day that Doppler broadened spectra were collected. The physical layout was such that Doppler and lifetime experiments could be performed simultaneously on the same sample.

All of the Doppler broadened spectra were deconvoluted and analysed by the DOPPFIT[10] computer program. In the method employed by this program, experimental data, i.e.

both the Doppler broadened spectrum and the resolution spectrum, are used directly without any data smoothing or assumption of any functional form for the spectra. A combination of an iterative technique and a curve fitting technique is employed whereby a model is introduced and fitted to the deconvoluted spectrum obtained by the iterations. The introduction of a model is necessary to accomplish the separation of the deconvoluted spectrum into its various momentum components. The usual model specified in this work was the sum of 3 Gaussians.

The output of the program includes a plot of deviations between the experimental Doppler spectrum and the result of convoluting the model with the resolution spectrum. The above deviations give a χ^2 value, which may be used as a test criterion in order to choose the best result, given in the form of FWHM values and intensities for the Gaussians.

Figure 3.1

Block Diagram for Doppler Set-up

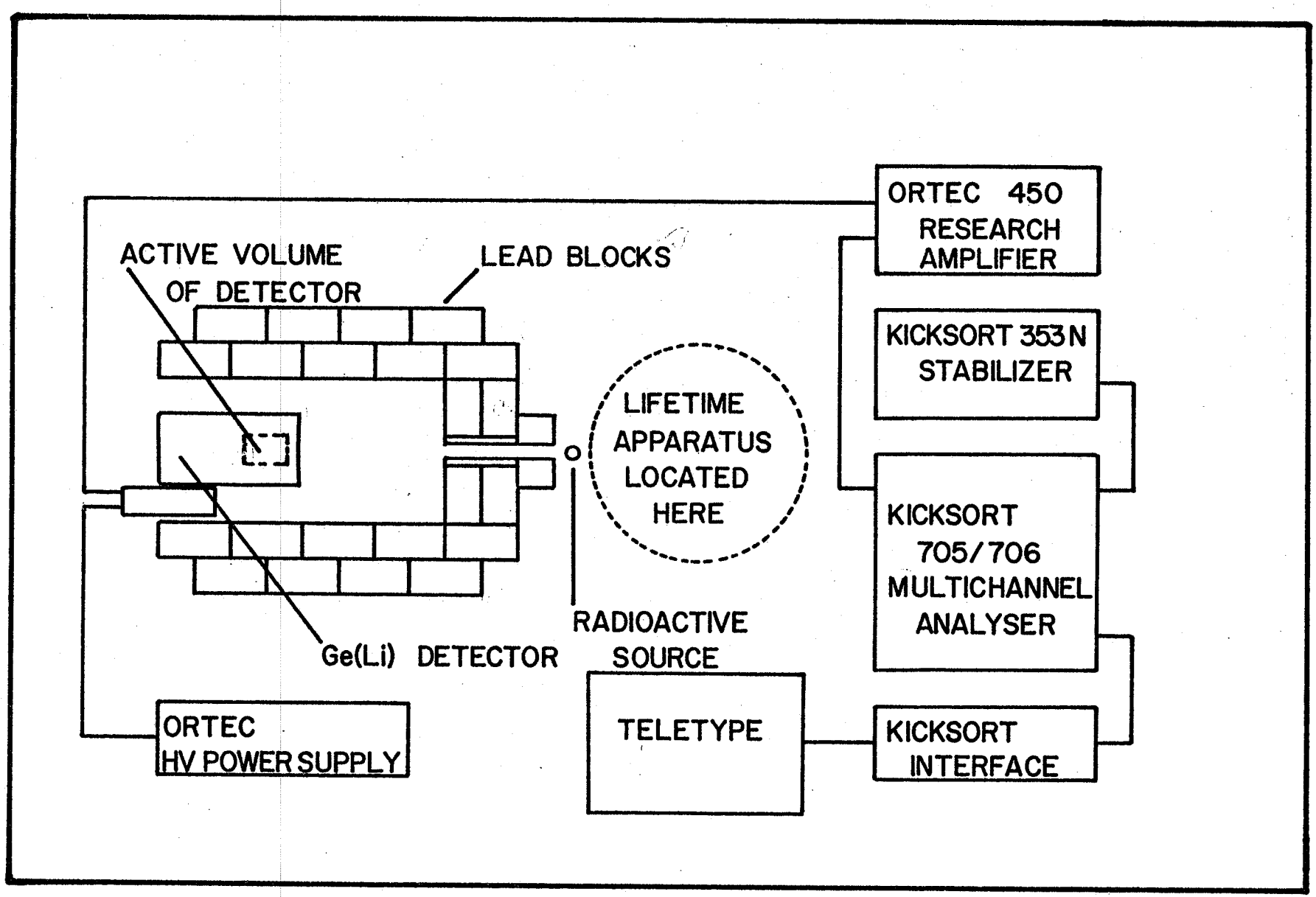
ACTIVE VOLUME
OF DETECTOR
LEAD BLOCKS
LIFETIME
APPARATUS
LOCATED
HERE
Ge(Li) DETECTOR
RADIOACTIVE
SOURCE
ORTEC 450
RESEARCH
AMPLIFIER
KICKSORT 353N
STABILIZER
KICKSORT
705/706
MULTICHANNEL
ANALYSER
ORTEC
HV POWER SUPPLY
TELETYPE
KICKSORT
INTERFACE

Figure 3.2

The Resolution Spectrum of ^{85}Sr

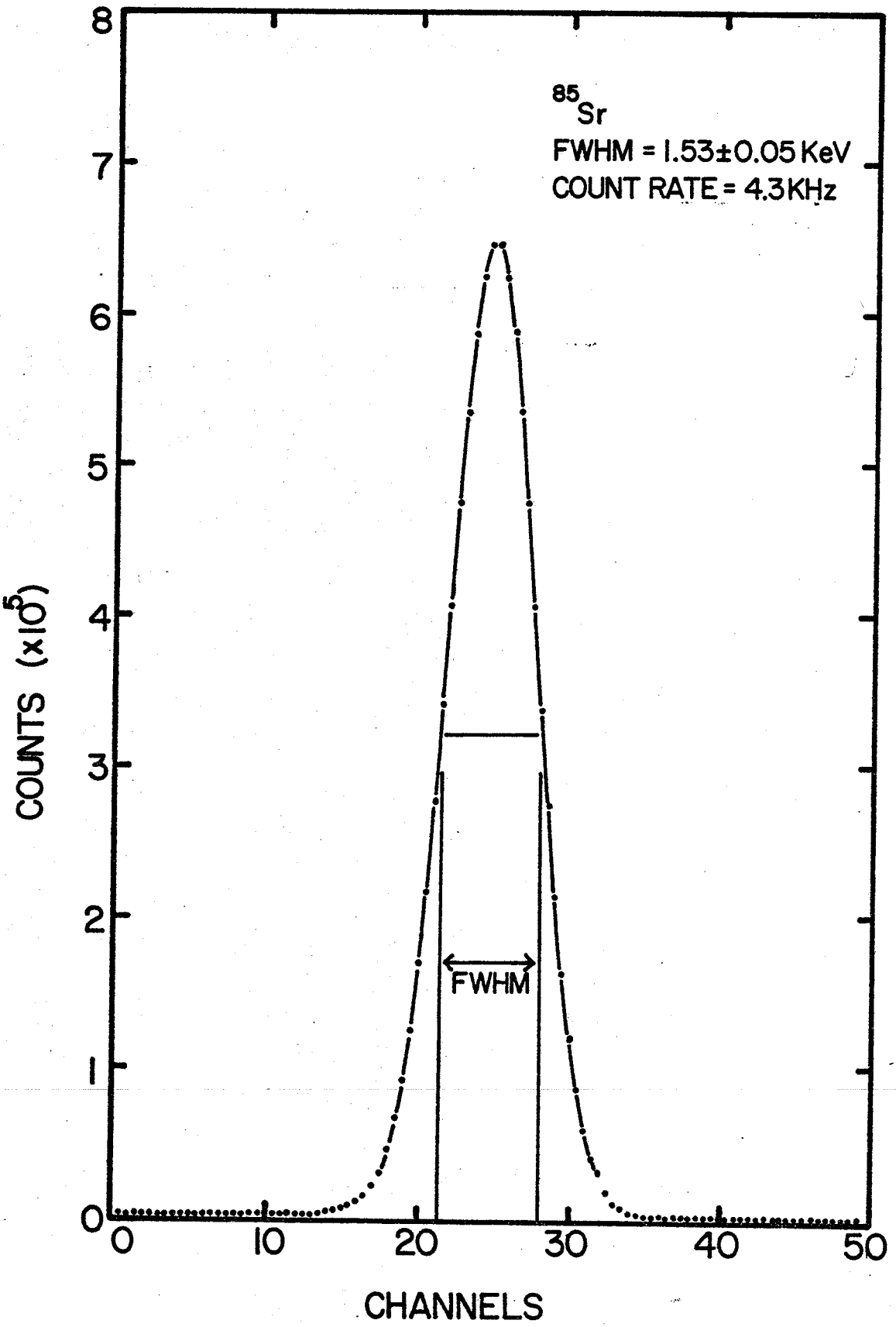
^{85}Sr
FWHM = 1.53±0.05 KeV
COUNT RATE = 4.3 KHz
FWHM
COUNTS (x10^5)
CHANNELS
0
1
2
3
4
5
6
7
8
0
10
20
30
40
50

3.2 The Lifetime Experiment

Standard and well established methods and equipment were used in the lifetime experiment. Figure 3.3 lists the model numbers of the equipment used. Contemporary lifetime experiments make use of the isotope ^{22}Na in which the emission of a positron is marked by the simultaneous emission of a 1.28 MeV gamma-ray. The system consists basically of two detectors, one to detect the 1.28 MeV nuclear gamma-ray (the "start" detector) and the other to detect one of the 0.511 MeV annihilation gamma-rays (the "stop" detector) and associated timing and energy selection electronics. Each detector has two outputs, one for timing purposes and one for energy selection. The time delay between "start" and "stop" pulses is converted by the TAC to a pulse whose amplitude is proportional to the time delay. Appropriate energy windows are set on the pulse height analysers so that emission and annihilation gamma-rays are recognized. If these gamma-rays are detected within 100 nsec of one another, the MCA gate is opened to accept the time information from the TAC.

The time resolution was measured with a ^{60}Co source with energy selection remaining the same as for ^{22}Na. Time spectra from ^{60}Co were accumulated in this manner for different instrumental settings until an optimum FWHM of this spectrum was achieved. Energy windows on the pulse height analysers for the 1.28 and 0.511 MeV gamma rays were

adjusted so that they were centred on the appropriate peaks of the energy spectrum. Energy window widths were calculated from the actual analyser dial settings. The values used for the 1.28 and 0.511 MeV windows were 30% and 40% respectively for the ratio of window width to the position of the lower edge of the window. A stable value of 330 psec for the FWHM was achieved. This value did not vary more than 2 psec over a period of 3 months. The FWHM was determined accurately by fitting a single Gaussian to the resolution spectrum in a least squares fashion.

The counting rate from a 15 μCi ^{22}Na source with window settings as described above was approximately 25 counts per second. Lifetime spectra were accumulated for periods of 800 minutes in most cases, to yield a total area in the spectrum of at least one million counts. For most samples, a minimum of 4 separate lifetime spectra were accumulated. A resolution spectrum was accumulated weekly.

All lifetime spectra were analysed with the computer program POSITRONFIT[21] or an extended version of POSITRONFIT[22]. The extended version of POSITRONFIT was tested with a spectrum generating program (see appendix I) which was designed to use an actual instrumental resolution function folded into the generated test curve which consisted of the sum of three exponential terms. Statistics were then introduced into the simulated spectrum which was subsequently analysed with the extended POSITRONFIT program. The input parameters (lifetimes and intensities) compared very favorably with

the parameters calculated by the analysis program. A summary of the results is contained in appendix I. The computer used for all the calculations was the University of Manitoba IBM 370/158.

Figure 3.3

Block Diagram for Lifetime Set-up

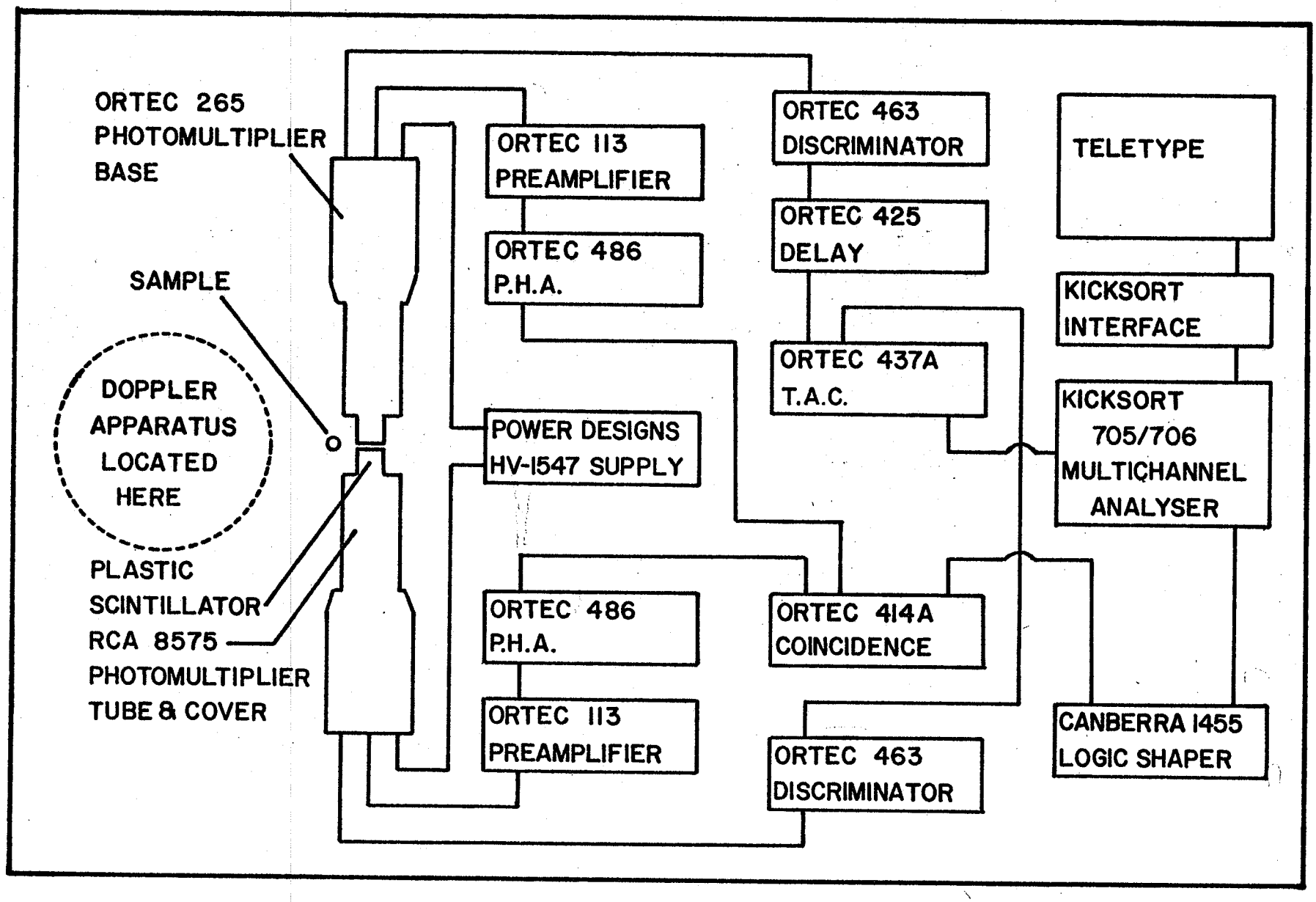
ORTEC 265
PHOTOMULTIPLIER
BASE
SAMPLE
DOPPLER
APPARATUS
LOCATED
HERE
PLASTIC
SCINTILLATOR
RCA 8575
PHOTOMULTIPLIER
TUBE & COVER
ORTEC 113
PREAMPLIFIER
ORTEC 486
P.H.A.
POWER DESIGNS
HV-1547 SUPPLY
ORTEC 486
P.H.A.
ORTEC 113
PREAMPLIFIER
ORTEC 463
DISCRIMINATOR
ORTEC 425
DELAY
ORTEC 437A
T.A.C.
ORTEC 414A
COINCIDENCE
ORTEC 463
DISCRIMINATOR
TELETYPE
KICKSORT
INTERFACE
KICKSORT
705/706
MULTICHANNEL
ANALYSER
CANBERRA 1455
LOGIC SHAPER

3.3 Source Construction

The main consideration in constructing a source for positron annihilation studies is to minimize the number of annihilations taking place in the source mount and source material itself. In the analysis of lifetime spectra by computer, it has usually been the practice to include a correction for annihilations in the source mount. Annihilations in the source material itself are usually negligible due to the use of very high specific activity sources. A typical source mount used by other investigators would be a thin mica sheet and the fraction of annihilations in the mount is as high as several percent. However, the exact number of annihilations in the source mount is quite uncertain, making the analysis of the lifetime spectrum much more difficult than if there were no source mount annihilations.

An actual calculation of the number of positrons stopped in the source mount is very difficult to perform because, in an actual experimental situation, the source is immersed in the sample liquid or sandwiched between slabs of the solid sample. In this case, there is backscattering into and through the source mount, and the number of resulting annihilations is difficult to estimate. The number of source mount annihilations may be estimated experimentally by observing the change in the shape of an accurately-known spectrum and correcting it in such a way as to restore it to its proper shape.

However, the best alternative is to design a source mount in which the fraction of annihilations is negligible.

In designing an ultra-thin source mount, material must be used with as low an atomic number as possible. Spanel, et al.[23] have studied the atomic number dependence of penetration of positrons through thin metallic foils. Their results show the importance of choosing a source mount with low atomic number to improve positron transmission. Therefore, aluminum is a suitable choice because of its relatively low atomic number of thirteen. The thinnest aluminum foil readily available has a thickness of 0.22 mg/cm^2. The results of Spanel, et al. show that for foil thicknesses below 10 mg/cm^2 the transmission curve takes on a highly non-exponential character, increasing more rapidly than an exponential for smaller thicknesses. Although the data points do not go below 3 mg/cm^2, they imply close to 100% transmission for a foil thickness of .22 mg/cm^2. Actual lifetime experiments on this foil[24] reveal that a change in the shape of the spectrum of silicon cannot be detected with fewer than 5 foils placed around the source. Based on this result, and with the use of only a single foil as a source mount, it is assumed that no source correction is necessary in the computer analysis of the lifetime spectra collected.

Design of a source mount with an ultra-thin foil for use in liquids, however, posed one minor difficulty. If a large rigid holder was used for the foil, it broke rather

easily when immersed in a liquid. Best results were obtained when the foil was held between two thin wire rings, 1 cm in diameter, and folded downwards over the bottom ring. These rings were formed in a continuous loop, soldered together in one spot, and the wire was extended upward and downward at right angles to the plane of the rings. (see figure 3.4). The source material was then deposited one drop at a time on the foil surface and allowed to evaporate. ^{22}NaCl dissolved in water with a specific activity of >100 μCi per μgram was used. Approximately 15 μCi of source material was used for each source constructed.

3.4 Sample Degassing

In the preparation of liquid samples for positron studies, it is imperative that the dissolved oxygen be removed. Even a very small amount of dissolved oxygen will drastically alter the lifetime of the long lived component. It was originally believed that the change in lifetime was due to ortho-to-para conversion by the paramagnetic oxygen.[25] Subsequently, it was found[26] that this is not the case and it has been suggested[27] that a chemical reaction between o-Ps and oxygen causes the shortening of the lifetime.

To remove the dissolved oxygen, the standard freeze-thaw technique was used. Great care was taken not to introduce any further impurities into the sample tubes which were constructed of glass (see figure 3.4). Sample tubes were first rinsed with concentrated sulfuric acid, then distilled water and heated by flame to a temperature just below the melting point of the glass. After cooling, the source was introduced into tube arm A and tube neck C was constricted with a propane torch to facilitate later sealing under vacuum. The liquid samples were introduced into arm B. Since a ground glass joint coated with vacuum grease was used to connect the sample tube to a degassing rack, care had to be taken not to allow the liquid sample to condense near the joint, dissolving the grease and contaminating the sample. In order to prevent this, a loose collar was constructed to fit over sample tube arm A and direct a

continuous flow of hot air from a heat gun upward. This prevented any condensation of liquid on the side of arm A during the degassing cycles.

The freeze-pump-thaw cycle was repeated until no dissolved gas bubbles escaped upon melting for two successive cycles. This entailed as many as fifteen cycles for some samples and as few as five for others. The sample tube was then sealed under vacuum with a torch while the sample in arm B was kept frozen by liquid nitrogen.

Figure 3.4

Construction of Radioactive Source and Sample Tube

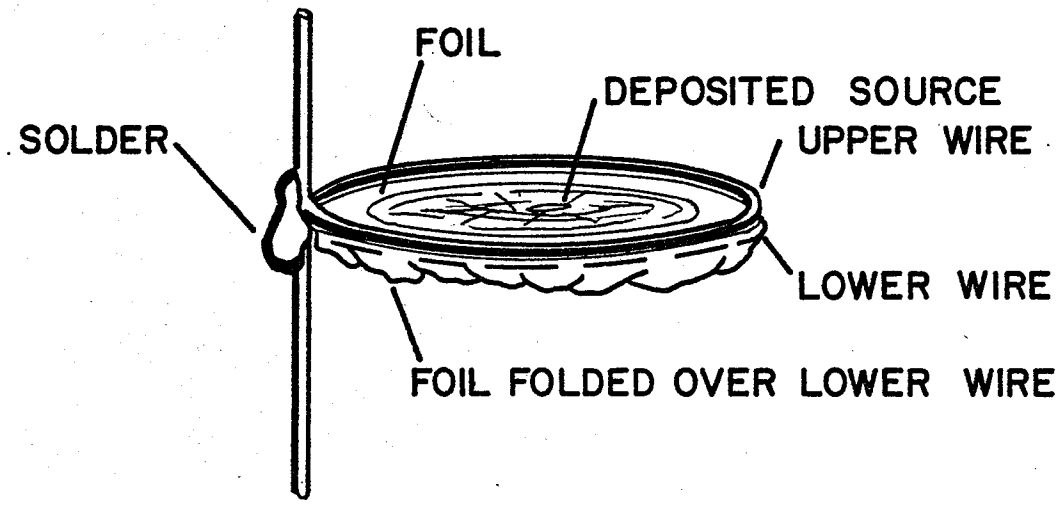
FOIL
DEPOSITED SOURCE
SOLDER
UPPER WIRE
LOWER WIRE
FOIL FOLDED OVER LOWER WIRE

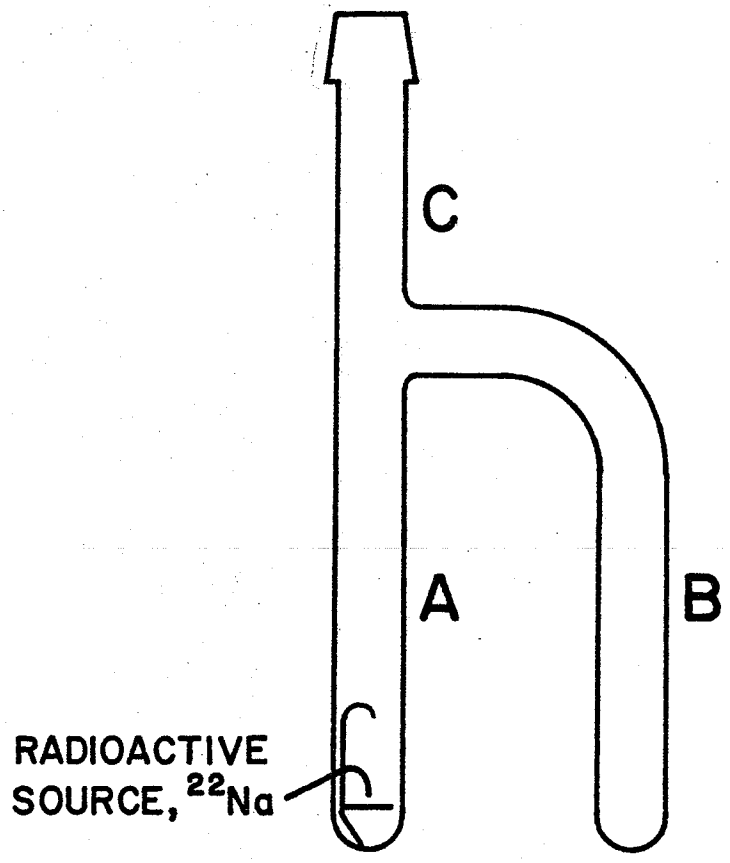
C
A
B
RADIOACTIVE
SOURCE, ^{22}Na

3.5 The Choice of Samples

A series of six-carbon hydrocarbons comprised the samples chosen. Three criteria were considered in the choice:

1. Since equation (2.61) shows that the surface tension is an important parameter in the bubble model, samples were chosen with a wide range of surface tensions.

2. To test the bubble model, the samples must be in the liquid state and, therefore, samples which are liquid at room temperature were selected.

3. Selection of samples was restricted to compounds having a reasonably high yield of Ps.

In addition, it was felt desirable to use a series of structural isomers to minimize the number of variables in the experiment, while at the same time, allowing, for example, for variations in the surface tension.

The compounds were all of highest purity commercially available, and no further purification was performed. The values of surface tension for some of the liquids were not available; these were measured by a standard capillary rise method.[28] In summary, the compounds, their surface tensions and purity, are listed in table 3.1.

TABLE 3.1

The Samples Used

SAMPLE	FORMULA	SURFACE TENSION* (dynes/cm)	PURITY
BENZENE	C_6H_6	28.65±0.05	Baker Analysed Spectroscopic Grade
HEXANE	C_6H_{14}	18.1±0.1	Aldrich Gold Label Spectroscopic Grade
2-METHYLPENTANE	C_6H_{14}	17.0±0.1†	Aldrich 99+%
3-METHYLPENTANE	C_6H_{14}	17.80±0.05	Aldrich 99+%
2,2-DIMETHYLBUTANE	C_6H_{14}	15.9±0.1	Aldrich 96%
2,3-DIMETHYLBUTANE	C_6H_{14}	17.1±0.1†	Aldrich 97%
1-FLUOROHEXANE	$C_6H_{13}F$	20.1±0.1	Eastman Not Specified
1-CHLOROHEXANE	$C_6H_{13}Cl$	25.73±0.05	Baker Grade
1-BROMOHEXANE	$C_6H_{13}Br$	27.8±0.1	Aldrich 99+%

* TEMPERATURE 23^0C

† Measured

Chapter IV

RESULTS AND DISCUSSION

4.1 The Doppler Spectra

The experimental Doppler spectra did not show any easily distinguishable features. Therefore, only a representative curve, that for hexane, is shown in figure (4.1) along with the deconvoluted result and the resolution spectrum. Although an attempt was first made to introduce a two Gaussian component model to describe the deconvoluted spectra, in most of the cases this resulted in large deviations between the input Doppler spectrum and the spectrum generated by convoluting the fitted Gaussians with the resolution spectrum. Hexane in the solid phase and 1-bromohexane were exceptions and two Gaussian components described their deconvoluted spectra well. All the other spectra were well described by the sum of three Gaussian components. This is in good agreement with the angular correlation results of Mogensen[29] who also employed three Gaussian components. The results of interest here (the width and intensity of the narrow component) were not sensitive to variation of the widest component.

Average values of the DOPPFIT results, i.e. full widths at half maximum (FWHM) and intensities of the Gaussian components together with the standard deviations in the mean were calculated for all the samples and are listed in table (4.1). In calculating these averages, any spectra exhibiting poor deviation plots in DOPPFIT (of the type described in section 3.1) were disregarded. The degree of reproducibility

of each result is indicated by the standard deviation. Actual uncertainties in the intensities of the various components are larger than the standard deviations due to a possible source of systematic error introduced by the use of a model in DOPPFIT. For instance, if one Gaussian fits the narrow component poorly at higher momentum values, then the wider components will be adjusted to compensate for this and the area of the narrow component will be systematically under or over-estimated. Thus the uncertainties in each intensity is conservatively estimated to be 10% of the value. Note that no narrow component data are listed for 1-bromohexane. The intensity is expected to be less than 2%, a value too small to be detected by the DOPPFIT program.

The results of the analyses performed by DOPPFIT may be interpreted as momentum distributions in accordance with equation (2.52) (using the data from table 4.1). When applied to a distribution with three components the required expression will take the form:

$$(4.1)\quad N_T(k) = \sum_{i=1}^{3} \frac{4I_i}{\sqrt{\pi}} \frac{k^2}{\sigma_i^3} \exp(-k^2/\sigma_i^2)$$

where $N_T(k)$ is the total momentum distribution and i = 1,2 and 3 refer to components A, B and C, respectively, in table (4.1). These distributions are plotted in figure (4.2) together with the corresponding angular correlation results[30] for three representative samples: benzene, hexane and 1-fluorohexane. It can be seen from the figure that the agreement between the two distributions is favorable. In addition,

more recent angular correlation results[29] for benzene and hexane analysed in terms of three Gaussians are in good agreement with the present results. Therefore, the Doppler broadening method in conjunction with DOPPFIT proves to be a suitable experimental technique.

Figure 4.1

Deconvolution of a Doppler Spectrum

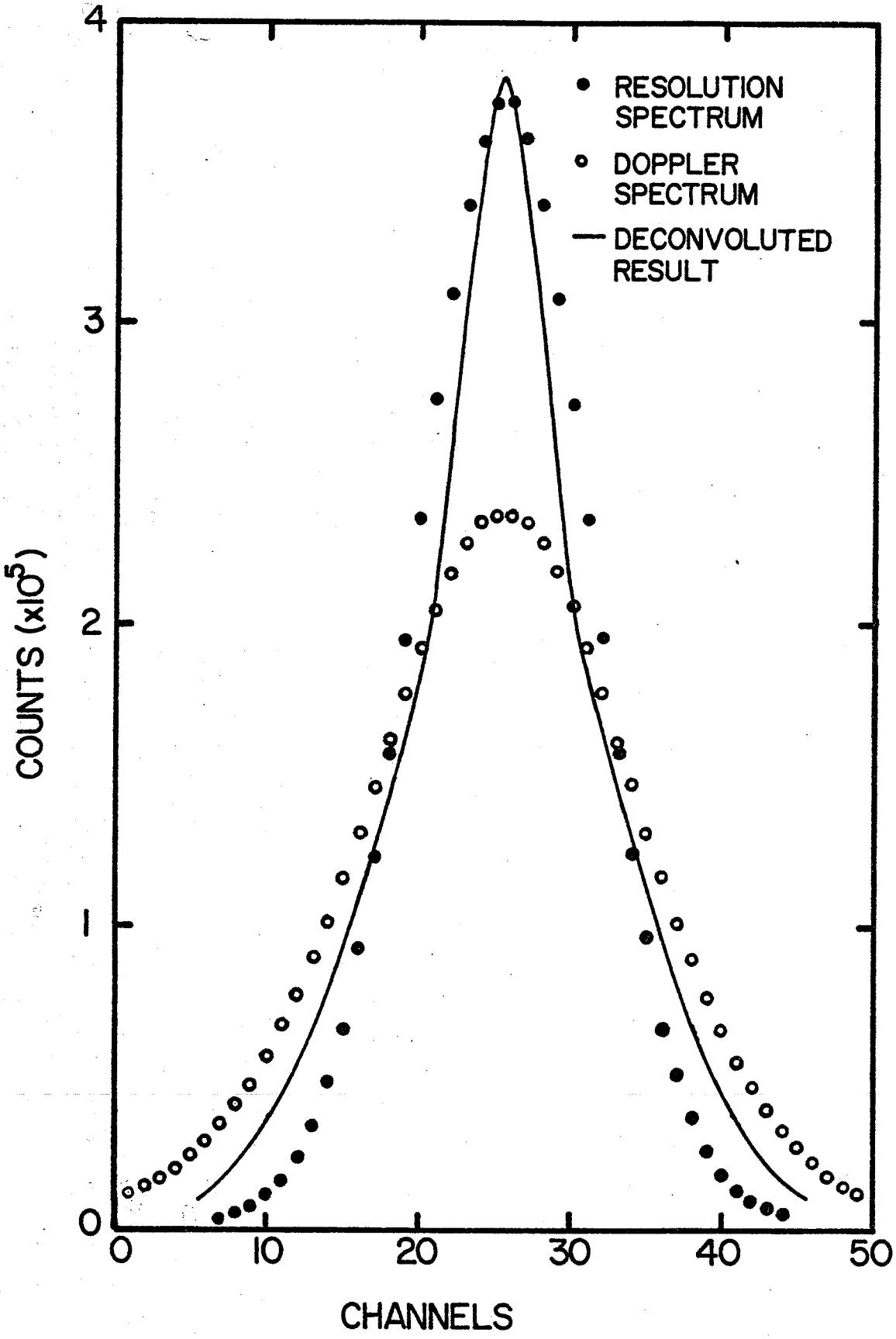
RESOLUTION SPECTRUM
DOPPLER SPECTRUM
DECONVOLUTED RESULT
COUNTS (x10^5)
CHANNELS
0
1
2
3
4
0
10
20
30
40
50

TABLE 4.1

Results for the Doppler Spectra

SAMPLE, TEMPERATURE	$FWHM_A$ (KeV)	I_A (%)	$FWHM_B$ (KeV)	I_B (%)	$FWHM_C$ (KeV)	I_C (%)
BENZENE, 23°C	0.77±0.05	13.9±0.7	2.16±0.01	78.7±0.6	4.3±0.6	7.4±0.1
BENZENE,-10°C(SOLID)	1.1±0.3	3±2	2.1±0.1	87±2	3.7±0.5	10±4
HEXANE,23°C	0.68±0.02	18.0±0.2	2.20±0.02	79.2±0.5	3.5±0.6	2.8±0.4
HEXANE,-196°C(SOLID)	0.9±0.1	1.6±0.8	2.25±0.01	98.4±0.8		
2-METHYLPENTANE,23°C	0.64±0.04	19.0±0.5	2.19±0.01	80.1±0.6	4.6±0.6	0.9±0.1
3-METHYLPENTANE,23°C	0.67±0.02	17.2±0.7	2.22±.01	81.5±0.6	6.2±0.6	1.3±0.1
2,2-DIMETHYLBUTANE,23°C	0.65±0.03	20±1	2.21±0.03	78±2	4.2±0.6	2±1
2,3-DIMETHYLBUTANE,23°C	0.67±0.03	17.4±0.9	2.20±0.01	81.2±0.7	5.6±0.6	1.4±0.3
1-FLUOROHEXANE,23°C	0.73±0.04	8.6±0.3	2.41±0.01	87.1±0.2	6.2±0.6	4.3±0.1
1-CHLOROHEXANE,23°C	0.8±0.1	4.8±0.8	2.23±0.01	94.4±0.9	9.2±0.6	0.8±0.1
1-BROMOHEXANE,23°C			2.15±0.01	96.4±0.2	5.5±0.6	3.6±0.2

Figure 4.2

Total Momentum Distributions in

a) Benzene ($23^{o}C$)

b) Hexane ($23^{o}C$)

c) 1-Fluorohexane ($23^{o}C$)

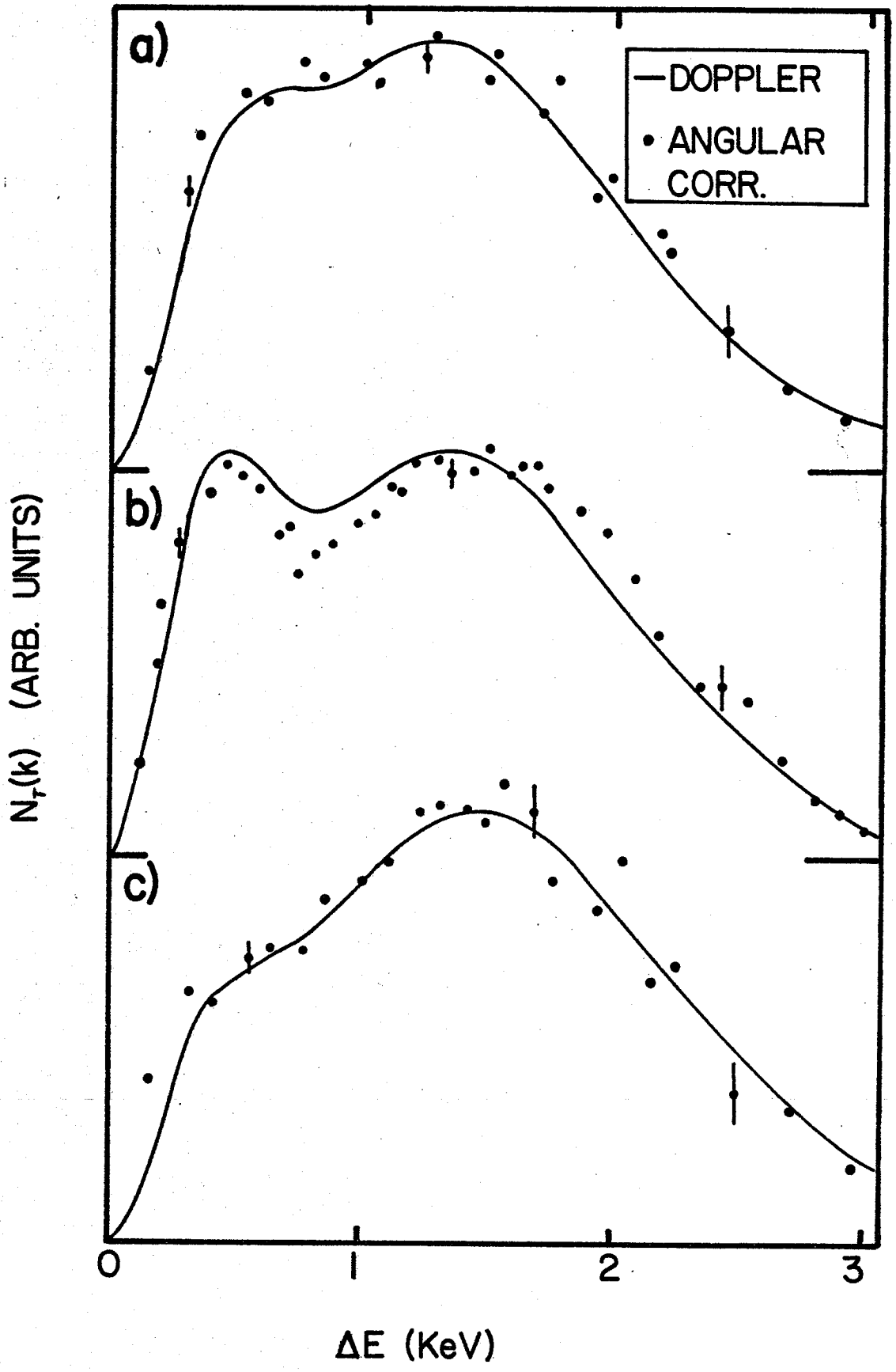
a)
b)
c)
—DOPPLER
• ANGULAR CORR.
$N_r(k)$ (ARB. UNITS)
0
1
2
3
ΔE (KeV)

4.2 The Lifetime Spectra

A representative lifetime spectrum, that for hexane, is shown in figure (4.3) along with the fitted spectrum from POSITRONFIT. An attempt was first made to specify two exponential components in POSITRONFIT, which, in most of the cases, resulted in a large variance between the experimental spectrum and the calculated spectrum. Benzene and hexane in the solid phase were exceptions, and two exponential components well described their lifetime spectra. All the other spectra were best described by three exponential components and POSITRONFIT was not able to detect four components in any of the spectra. This is different from the results of most previous work in liquids where the techniques have been capable of resolving only two components. Average values of the POSITRONFIT results in terms of mean lifetime τ, and intensity I together with the standard deviations in the mean were calculated for all the samples and are presented in table (4.2).

Figure 4.3

The Lifetime Spectrum of Hexane

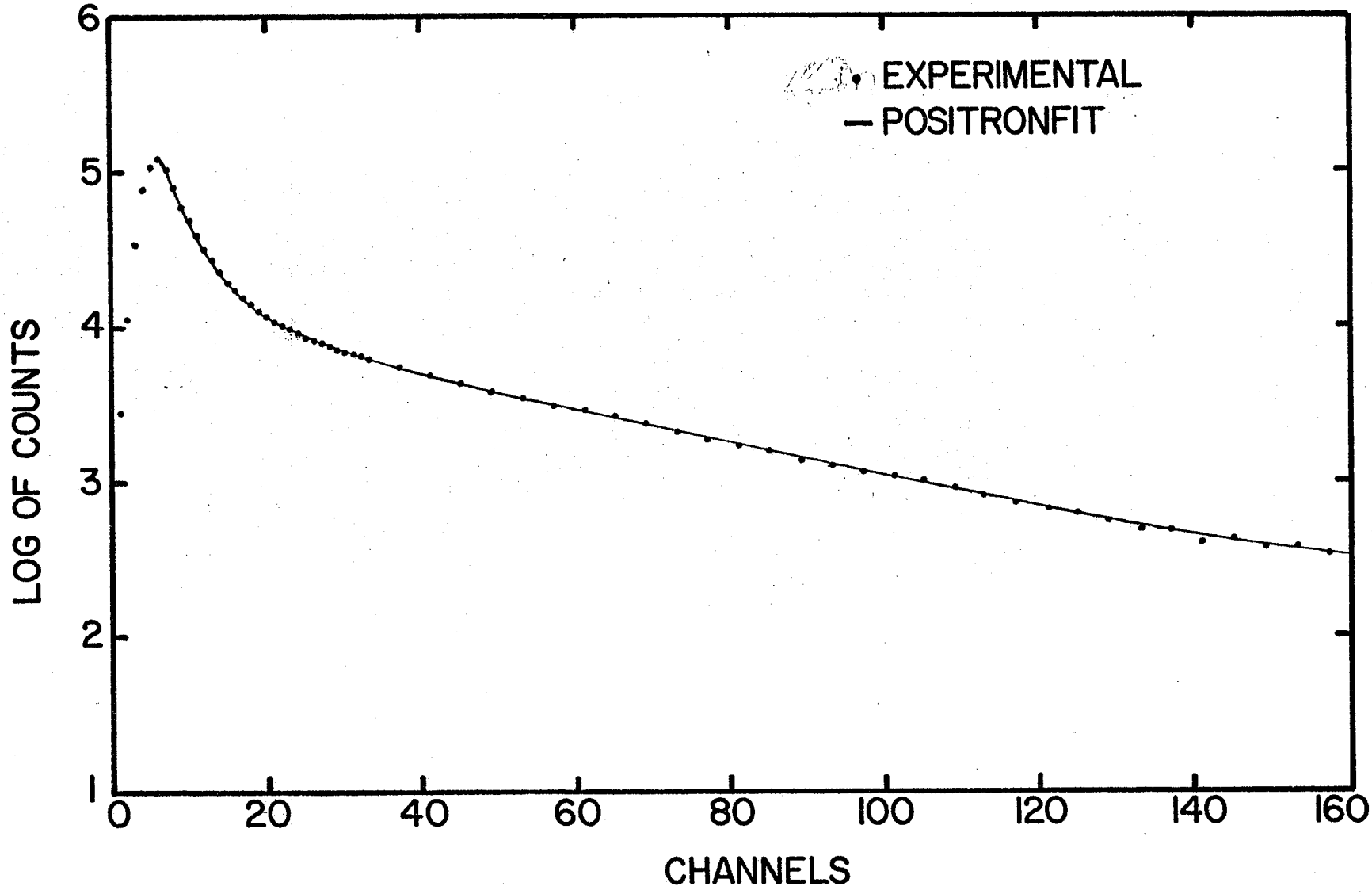
EXPERIMENTAL
POSITRONFIT
LOG OF COUNTS
CHANNELS
6
5
4
3
2
1
0
20
40
60
80
100
120
140
160

TABLE 4.2

Results for the Lifetime Spectra

SAMPLE, TEMPERATURE	τ_1 (nsec)	I_1 (%)	τ_2 (nsec)	I_2 (%)	τ_3 (nsec)	I_3 (%)
BENZENE, 23°C	0.18±0.02	28±2	0.46±0.02	33.4±1.5	3.23±0.01	38.9±0.7
BENZENE, -10°C (SOLID)			0.33±0.01	70.6±0.5	1.50±0.01	29.4±0.5
HEXANE, 23°C	0.18±0.01	23±2	0.48±0.01	36.7±0.8	3.94±0.06	40.7±1.8
HEXANE, 23°C (SOLID)			0.32±0.01	80±1	1.31±0.06	20±1
2-METHYLPENTANE, 23°C	0.18±0.01	21.2±0.6	0.48±0.01	36.5±0.6	4.20±0.02	42.3±0.1
3-METHYLPENTANE, 23°C	0.19±0.02	24±2	0.49±0.02	34±2	4.04±0.05	42.2±0.2
2,2-DIMETHYLBUTANE, 23°C	0.15±0.01	31±3	0.48±0.01	30±1	4.50±0.01	39±3
2,3-DIMETHYLBUTANE, 23°C	0.17±0.01	20.9±0.6	0.47±0.01	36.1±0.7	4.20±0.02	43.0±0.1
1-FLUOROHEXANE, 23°C	0.25±0.04	29±8	0.49±0.02	52±8	3.60±0.03	18.5±0.1
1-CHLOROHEXANE, 23°C	0.30±0.04	28±18	0.48±0.04	58±18	3.12±0.04	13.8±0.2
1-BROMOHEXANE, 23°C	0.27±0.04	40±13	0.50±0.04	54±12	2.49±.07	5.4±0.6

4.3 Doppler Spectra and the Bubble Model

As stated previously, the narrow or low momentum component of the Doppler broadened spectrum is due to the annihilation of p-Ps. Section (2.3) suggests a procedure for application of the bubble model theory to the narrow component of the deconvoluted Doppler spectrum in the case where the narrow component is described by a Gaussian. Accordingly, the FWHM values for the narrow component from table (4.1), ($FWHM_A$), were used to calculate σ values with relation(2.51), (where σ is the Gaussian width parameter). Then expression (2.49), describing the theoretical prediction was fitted to (2.52), thus describing the experimental result in terms of k_1R and R. The fitting procedure used a simple two parameter least square technique. The parameters K_1R and R in (2.49) were varied to form a grid of variances and the values giving the minimum variance was chosen. This was performed to an accuracy of 0.1% on the k_1R and R values. Appendix II lists the computer program used. The variances converged smoothly to a best value with no local minima appearing. Table (4.3) summarizes the values of k_1R and R given by the fit along with the σ values for each sample. The results of the fitting are shown graphically in figure (4.4) with the theoretical fits represented by solid lines and the experimental data (on the basis of Gaussians) by dots. In all cases the curves could not be distinguished from the dots, within plotting error. All the curves fit the data within

0.5% in the peak of the momentum distribution (i.e. at 1σ value), with the exception of benzene, 1-fluorohexane and 1-chlorohexane which deviated by less than 1% at the peak. Up to 1.5σ all the curves fit the data within 1%. At higher values of momentum the theoretical curve fell below the experimental points. Agreement between the two distributions is remarkable considering that some degree of approximation was involved in fitting a Gaussian to the narrow component (in DOPPFIT) as a means of describing the experimental data. The validity of the bubble model theory is supported by this agreement.

As indicated in table (4.1), two samples (hexane and benzene) were investigated in the solid phase. One reason for this investigation was to check on earlier angular correlation results[31] where radiation damage due to the large positron source was suspected. The current results agree with the angular correlation experiment in that the narrow component is essentially non-existent in spite of the indications from the lifetime results that positronium is formed. In addition, if the bubble model is correct for liquids, one would expect significantly different results in the solid phase. These results are therefore included simply to exhibit this difference and are not discussed further.

TABLE 4.3

Results of the Theoretical Fit

to the Low Momentum Component

SAMPLE	σ (KeV) (EXP.)	R(Å) (FIT)	$k_1 R$ (FIT)
BENZENE	0.46±0.03	3.9±0.3	2.52±0.02
HEXANE	0.41±0.01	4.4±0.1	2.52±0.02
2-METHYLPENTANE	0.39±0.02	4.6±0.2	2.52±0.02
3-METHYLPENTANE	0.40±0.01	4.5±0.1	2.52±0.02
2,2-DIMETHYLBUTANE	0.39±0.02	4.6±0.2	2.52±0.02
2,3-DIMETHYLBUTANE	0.40±0.02	4.5±0.02	2.52±0.02
1-FLUOROHEXANE	0.44±0.02	4.1±0.2	2.52±0.02
1-CHLOROHEXANE	0.48±0.06	3.7±0.4	2.52±0.02

Figure 4.4

Theoretical & Experimental Momentum Distributions for p-Ps

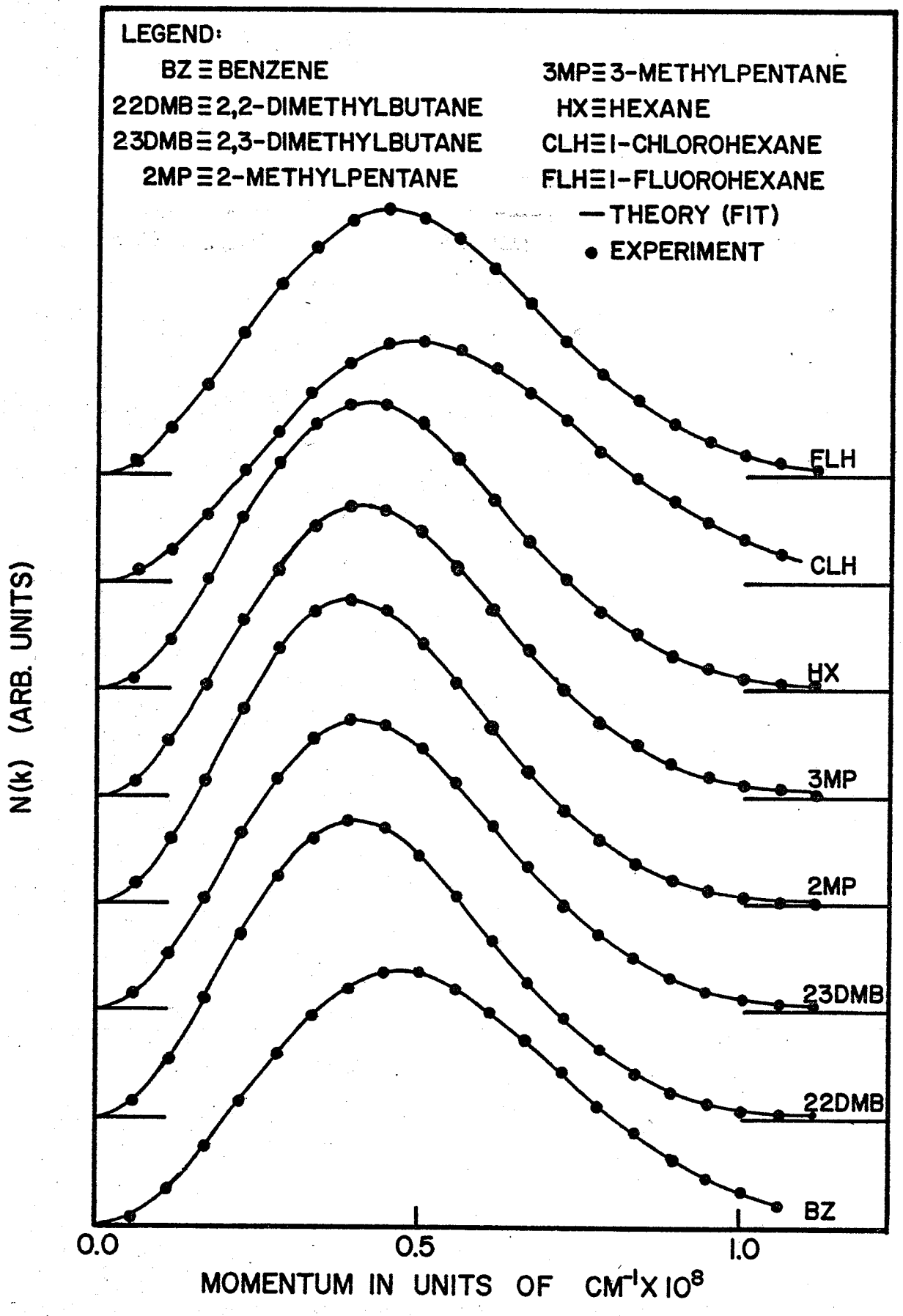
LEGEND:
BZ ≡ BENZENE
22DMB ≡ 2,2-DIMETHYLBUTANE
23DMB ≡ 2,3-DIMETHYLBUTANE
2MP ≡ 2-METHYLPENTANE
3MP ≡ 3-METHYLPENTANE
HX ≡ HEXANE
CLH ≡ 1-CHLOROHEXANE
FLH ≡ 1-FLUOROHEXANE
— THEORY (FIT)
• EXPERIMENT
FLH
CLH
HX
3MP
2MP
23DMB
22DMB
BZ
N(k) (ARB. UNITS)
0.0
0.5
1.0
MOMENTUM IN UNITS OF CM⁻¹ X 10⁸

4.4 The Bubble Model and the Lifetime Spectra

As stated previously, the long lived component of the lifetime spectrum is due to the pickoff annihilation of o-Ps in the case where Ps is formed. In section (2.4) equation (2.57) relates the parameter k_1R in the bubble model to the observed annihilation rate. Equation (2.57) is repeated here for the sake of convenience:

$$(2.57)\quad \lambda_{obs}-\lambda_{vac} = \pi r_0^2 c\rho_0 \left(\frac{\sin^2(k_1R)}{1-k_1R\cot(k_1R)}\right),$$

where r_0 is the classical electron radius, c the speed of light in a vacuum and ρ_0 the effective number of electrons per unit volume. The parameter ρ_0 may be determined with the assumption that the positron will annihilate only with electrons in the outermost shell of each of the constituent atoms of the molecule. Then,

$$(4.2)\quad \rho_0 = \frac{N_A \rho Z}{m}$$

where N_A is Avogadro's number, ρ the density, m the molecular weight and Z the total number of electrons in the outermost shells of the constituent atoms of each molecule. One may solve for k_1R by computer if all the other parameters are known. For instance, $\lambda_{obs} = \lambda_3 = {}^1/_{\tau_3}$ from table(4.2). In this work the "bisection" method was employed to solve for k_1R and is described in Appendix III.

In section 2.5 k_1R is related to the bubble radius,R, and to the surface tension, γ, by relation (2.62) in which the parameter Z_0 is set equal to zero. Given that k_1R has

been calculated by the method described above and that γ is known, the bubble radius, R, may be calculated. Table (4.4) lists some of the parameters and the results of these calculations. The uncertainties shown reflect the uncertainties in the experimental values of λ_{obs}, and do not take into account for example, the uncertainty in assigning to Z the number of valence electrons.

TABLE 4.4

Bubble Model Parameters From The Lifetime Results

SAMPLE	Z	$\gamma \left(\frac{\text{dynes}}{\text{cm}}\right)$	λ_{obs} ($nsec^{-1}$)	$k_1 R$	R (Å) ($Z_0=0$)
BENZENE	30	28.65±0.05	0.309±0.001	2.274±0.001	4.12±0.01
HEXANE	38	18.1±0.1	0.254±0.004	2.290±0.005	4.65±0.05
2-METHYLPENTANE	38	17.0±0.1	0.238±0.001	2.306±0.001	4.76±0.02
3-METHYLPENTANE	38	17.80±0.05	0.247±0.003	2.300±0.003	4.69±0.05
2,2-DIMETHYLBUTANE	38	15.9±0.1	0.222±0.001	2.325±0.001	4.88±0.02
2,3-DIMETHYLBUTANE	38	17.1±0.1	0.238±0.001	2.310±0.001	4.76±0.02
1-FLUOROHEXANE	44	20.1±0.1	0.277±0.002	2.307±0.002	4.57±0.05
1-CHLOROHEXANE	44	25.73±0.05	0.320±0.004	2.247±0.004	4.18±0.06
1-BROMOHEXANE	44	27.8±0.1	0.40±0.01	2.167±0.009	3.95±0.06

4.5 Comparison of the Bubble Model Applications

The parameters R and k_1R arising when the bubble model is applied to the Doppler and lifetime results as tabulated in tables (4.3) and (4.4) are compared directly in table (4.5). Examination of the R values shows a definite correlation, and therefore some support for the bubble, but the values from the lifetime results are consistently higher by approximately 5% (more in the case of 1-fluorohexane and 1-chlorohexane). The k_1R parameters from the Doppler results are consistently higher than the corresponding lifetime parameters by approximately 9%. Another feature of the Doppler k_1R parameters is their constancy compared to the variation of the lifetime k_1R parameters. This constancy may reflect the constant general shape of the Gaussian describing the narrow part of the experimental counting rate distribution.

An interpretation of these results is possible with the realization that the parameters R and k_1R are related to the centre of mass momentum of the Ps. An expectation value for the Ps momentum, $\langle k \rangle$ may be simply calculated from the kinetic energy (K.E.) of the Ps. The K.E.'s of the Ps inside and outside the bubble are known since the total energy of the Ps is E at all times (this is the eigenvalue for the Hamiltonian in the bubble model) and the potential energy is zero inside the bubble and V_0 outside the bubble. The value of the K.E. of the Ps will vary depending on whether

TABLE 4.5

Comparison of Bubble Model Parameters

SAMPLE	R (Doppler)	k_1R (Doppler)	R (Lifetime)	k_1R (Lifetime)
BENZENE	3.9±0.3	2.52±0.02	4.12±0.01	2.274±0.001
HEXANE	4.4±0.1	2.52±0.02	4.65±0.05	2.290±0.005
2-METHYLPENTANE	4.6±0.1	2.52±0.02	4.76±0.02	2.306±0.001
3-METHYLPENTANE	4.5±0.1	2.52±0.02	4.69±0.05	2.300±0.003
2,2-DIMETHYLBUTANE	4.6±0.1	2.52±0.02	4.88±0.02	2.325±0.001
2,3-DIMETHYLBUTANE	4.5±0.1	2.52±0.02	4.76±0.02	2.310±0.001
1-FLUOROHEXANE	4.1±0.2	2.52±0.02	4.57±0.02	2.307±0.002
1-CHLOROHEXANE	3.7±0.4	2.52±0.02	4.18±0.02	2.247±0.004

it is inside the well or outside the well. The probabilities for being inside and outside the well, P_1 and P_2 respectively, are known from equation (2.55) and since $P_1 + P_2 = 1$. Thus the expectation value for the momentum is

$$(4.3) \quad \langle k \rangle = k_1 P_1 + k_2 P_2$$

where k_1 (it is shown below that this is the factor k_1 in $k_1 R$) is the momentum inside the bubble and k_2 is the momentum outside the bubble. The parameters k_1 and k_2 as previously defined in Chapter 2 are recognized as the required momenta since

$$(4.4) \quad k_1 = \sqrt{\frac{4mE}{\hbar^2}} \quad \text{and}$$

$$(4.5) \quad k_2 = \sqrt{\frac{4m(V_0 - E)}{\hbar^2}}$$

(i.e. each is of the required form to yield a k_1 and k_2 in the momentum units of length^{-1}). Then, making use of the fact that (2.20) gives a relationship between k_1 and k_2 one may write

$$(4.6) \quad \langle k \rangle R = k_1 R - \frac{(k_1 R)\ \sin^2(k_1 R)\,(1+\cot(k_1 R))}{1-(k_1 R)\cot(k_1 R)}$$

This allows one to determine $\langle k \rangle$ where $k_1 R$ and R are known. Substitution of $k_1 R$ and R from the Doppler results into (4.6) yields a higher $\langle k \rangle$ than does substitution of $k_1 R$ and R from lifetime results. In order to still maintain a consistent picture of the bubble model in view of both the Doppler and lifetime results the following explanation is suggested. The prediction of a higher momentum in the Doppler case may be due to the mixing of a higher momentum state with the normal

bubble state. For example, some bubble states may be excited 2s states or some Ps may be in a second type of bound state such as a chemically bound state with ions or molecules where the degree of localization of the Ps may be greater resulting in a higher centre of mass momentum. The excited state type of explanation for an apparently too high value of Ps centre of mass momentum was first advanced by Hernandez and Choi[32] in the case of angular correlation results for liquid helium. They expressed the observed Ps state as a combination of a normal state and an excited state. In the present case, the fact that the second state is not observed in the lifetime result (where use is made of only the longest lived component) would be due to a different pickoff rate in this state since the penetration of the Ps wave function into the medium would be different in a higher energy state. The supposition of the presence of an excited state may be examined upon calculations of the various parameters for all allowed bubble s states. It is assumed that the k_1R and R values from the lifetime data result only from the ground state of the bubble and therefore may be used to calculate the potential well depth, V_0, from equation (2.21). This value, and the surface tension, γ, serve as input parameters in the graphical solution of equation (2.61) with $Z_0 = 0$, yielding a value of k_1R. The calculation employs the method of Appendix III. Equation (2.21) is then used to calculate the R values for the allowed bound state solutions.

Significantly, this calculation does allow a weakly bound excited state for the bubble. The excited state parameters along with the potential well depths are listed in table (4.6). Therefore, in the analyses of the Doppler results the wave function for the 1s state was used to describe what may be a mixture of 1s and 2s states. It is difficult to say how the parameter k_1R from the Doppler result should behave in this type of situation. However, the behavior of the parameter R calculated from the Doppler result may be understood if the following simple picture is considered. Assuming a fraction P of Ps to be in the 1s state and 1-P to be in the 2s state, then as a crude approximation R from the Doppler result (referred to as $\bar{R}$) could be expressed as a weighted average of the 1s and 2s values for R. Table (4.7) contains the values of P calculated according to the above assumption. The fact that this estimation of P gives a regular, reasonable value ($P \simeq 0.90$) increases the possibility that the above is a correct explanation of the difference between the Doppler and lifetime results. Nevertheless, the presence of a second type of bound state for some of the Ps also remains as a possible explanation for the difference in calculated bubble model parameters for the Doppler and lifetime experimental results. Bound states of the type required here have been postulated and observed by investigators in the area of Ps chemistry.[1A] Many of these bound states of Ps in atomic molecular and ionic systems, such as PsH, PsCl, etc.

are stable and may have binding energies of approximately 1 eV. It is conceivable that the mixing of such a state with the low momentum Doppler component could result in a higher calculated centre of mass momentum and a higher degree of localization (lower R) in the Doppler case. However, the chemically bound state is apparently not as probable as the 2s state since no independent evidence has been discovered to support its formation, whereas in the case of the 2s bubble state there is already strong evidence for the presence of the 1s state.

TABLE 4.6

Excited State Parameters

SAMPLE	V_0 (eV)	E_{1S} (eV)	E_{2S} (eV)	k_1R	R(Å)
BENZENE	0.99	0.58	0.98	1.654	2.30
HEXANE	0.82	0.46	0.81	0.646	2.52
2-METHYLPENTANE	0.81	0.45	0.80	1.642	2.53
3-METHYLPENTANE	0.82	0.46	0.81	1.644	2.51
2,2-DIMETHYLBUTANE	0.81	0.43	0.80	1.637	2.52
2,3-DIMETHYLBUTANE	0.82	0.45	0.81	1.641	2.51
1-FLUOROHEXANE	0.88	0.49	0.87	0.643	2.42
1-CHLOROHEXANE	0.90	0.55	0.89	1.663	2.43

TABLE 4.7

Proportions of 1s and 2s States

SAMPLE	R_{1s}	R_{2s}	$\bar{R}$	P
BENZENE	4.12	2.30	3.9	0.87
HEXANE	4.65	2.52	4.4	0.88
2-METHYLPENTANE	4.76	2.53	4.6	0.93
3-METHYLPENTANE	4.69	2.51	4.5	0.91
2,2-DIMETHYLPENTANE	4.88	2.52	4.6	0.88
2,3-DIMETHYLBUTANE	4.76	2.51	4.5	0.88
1-FLUOROHEXANE	4.57	2.42	4.1	0.78
1-CHLOROHEXANE	4.18	2.43	3.7	0.73

4.6 Relationships Between the Various Component Intensities

It is possible to establish general relationships between the various component intensities for both the lifetime and Doppler results. For example, since 3/4 of the Ps is o-Ps and 1/4 is p-Ps, it would be expected that the intensity, I_3, of the long lived component and the intensity, I_A, of the low momentum Doppler component should be simply related. The assumption here is that I_3 is due to o-Ps pickoff and I_A is due to p-Ps. Since the p-Ps also undergoes pickoff by the same mechanism as the o-Ps, a small fraction of it will not annihilate with low centre of mass momentum. One may argue that the fractional change of low momentum events due to the pickoff rate, λp, is equal to the ratio of the actual annihilation rate of p-Ps, $\lambda p + \lambda_0$, to the annihilation rate λ_0 which would occur if there were no pickoff. Then one may calculate a predicted intensity, I_A', of parapositronium with

$$(4.7) \quad I_A' = I_A \frac{\lambda p + \lambda_0}{\lambda_0}$$

where λp is the pickoff rate and λ_0 is the p-Ps vacuum self annihilation rate of $1/.125$ nsec^{-1}. Furthermore, it is also assumed that I_1, the shortest lived component, contains the p-Ps annihilations. Thus, if I_3 consisted of all the o-Ps annihilations and I_1 consisted of only p-Ps annihilations then the following relationships should hold:

$$(4.8) \quad I_1 = I_A' = I_3/3 \ .$$

The values of I_1, I_A' and $I_3/3$ are tabulated in table (4.8). The uncertainties in $I_1$and I_3 are taken to be the standard deviations in the calculated mean values. Inspection of table (4.8) shows that relation (4.8) is not valid (although one could allow $I_A' = I_3/3$, within uncertainty, for benzene and 1-chlorohexane). A valid relationship on the basis of table (4.8) is

$$(4.9) \quad I_1 > I_A' > I_3/3 \ .$$

This complete relationship has not previously been observed in the case of organic liquids, primarily because computational and experimental techniques have only recently been able to resolve 3 components in the lifetime spectra or clearly resolve the narrow component in angular correlation distributions or Doppler spectra.

As a result of relation (4.9) it becomes necessary to search for a mechanism which increases I_1 and I_A' relative to I_3. Three possible explanations of (4.9) are proposed in this work. First, the possibility is considered that there is a transition from the bubble state to another state (e.g. a chemically bound state) where the pickoff rate is much greater resulting in some of the o-Ps being included with I_1 instead of with I_3. Second, the possibility of ortho to para spin conversion is considered which would increase I_1 and I_A' at the expense of I_3. Finally, it is proposed that some of the positronium follows a separate branch and does not form the bubble, instead forming a bound state (e.g. an

excited bubble state or a chemically bound state) with a much greater pickoff rate and therefore is included with I_1. These three proposals are presented in detail and tested in the following sections.

TABLE 4.8

Relationships Among Various Intensities

SAMPLE	I_1 (%)	I'_L (%)	$I_3/3$ (%)
BENZENE	28±2	14±1	13.0±0.2
HEXANE	23±2	19±2	13.6±0.6
2-METHYLPENTANE	21±1	20±2	14.10±0.05
3-METHYLPENTANE	24±2	18±2	14.1±0.1
2,2-DIMETHYLBUTANE	31±3	21±2	13.0±1.0
2,3-DIMETHYLBUTANE	21±1	18±2	14.33±0.05
1-FLUOROHEXANE	29±8	9±1	6.17±0.05
1-CHLOROHEXANE	28±18	5±1	4.6±0.2
1-BROMOHEXANE	40±13	†	1.8±0.2

4.7 The "Transition" Model

In the "transition" model it is proposed that positronium undergoes a transition from the bubble (state $[n_1]$) and becomes chemically bound in the medium (state $[n_2]$). The analysis of this situation is similar to the method of West[33] and proceeds as follows.

Consider the schematic diagram for this reaction as it applies to o-Ps:

$$2\gamma \xleftarrow{\lambda_1^0} [n_1] \xrightarrow{K_{12}} [n_2] \xrightarrow{\lambda_2^0} 2\gamma$$

where $\lambda_1^0 = \lambda_{vac} + \lambda_p$ and $\lambda_2^0 = \lambda_{vac} + \lambda_c$ (λc is the pickoff rate in the chemically bound state), K_{12} is the reaction rate constant and 2γ refers to annihilation. It is assumed that the reverse reaction rate constant, $K_{21} = 0$. At $t = 0$, the states $[n_1]$ and $[n_2]$ have populations n_0 and zero, respectively. These populations change with time and their rates of change are given by

$$(4.10) \quad \frac{dn_1}{dt} = -(\lambda_1^0 + K_{12})n_1$$

and

$$(4.11) \quad \frac{dn_2}{dt} = K_{12} n_1 - \lambda_2^0 n_2 .$$

The eigenvalues Λ_i of this system are given by

$$(4.12) \quad (-1)^2 \begin{vmatrix} -(\lambda_1^0 + K_{12}) - \Lambda & 0 \\ K_{12} & -\lambda_2^0 - \Lambda \end{vmatrix} = 0,$$

which yields

$$(4.13)\quad \Lambda_1 = -(\lambda_1^0 + K_{12})$$

and

$$(4.14)\quad \Lambda_2 = -\lambda_2^0 .$$

The general solution is then given by

$$(4.15)\quad n_1 = A \exp -(\lambda_1^0 + K_{12})t + B \exp -\lambda_2^0 t$$

and

$$(4.16)\quad n_2 = C \exp -(\lambda_1^0 + K_{12})t + D \exp -\lambda_2^0 t.$$

The constants A, B, C and D may be determined from the following four initial conditions:

$$(4.17)\quad n_1(0) = n_0$$

$$(4.18)\quad n_2(0) = 0$$

$$(4.19)\quad \frac{dn_1}{dt}(t=0) = -(\lambda_1^0 + K_{12})n_1(0)$$

$$(4.20)\quad \frac{dn}{dt}(t=0) = K_{12} n_1(0) - \lambda_2^0 n_2(0)$$

This results in

$$(4.21)\quad A = n_0$$

$$(4.22)\quad B = 0$$

$$(4.23)\quad C = \frac{-n_0 K_{12}}{\lambda_1^0 + K_{12} - \lambda_2^0}$$

$$(4.24)\quad D = \frac{n_0 K_{12}}{\lambda_1^0 + K_{12} - \lambda_2^0} .$$

Then the rate of annihilations from each state is

$$(4.25)\quad \frac{-dn_1}{dt} = n_0(\lambda_1^0 + K_{12})\exp-(\lambda_1^0 + K_{12})t$$

$$(4.26)\quad \frac{-dn_2}{dt} = \frac{n_0(\lambda_1^0 + K_{12})K_{12}}{\lambda_2^0 - (\lambda_1^0 + K_{12})} \exp-(\lambda_1^0 + K_{12})t$$

$$\frac{-n_0 \lambda_2^0 K_{12}}{\lambda_2^0 - (\lambda_1^0 + K_{12})} \exp-\lambda_2 t$$

The contribution to the experimental lifetime spectrum by

decay from states $[n_1]$ and $[n_2]$ will be

$$(4.27) \quad n(\bar{t}) = \int_{t_1}^{t_2} \left(-\frac{dn_1}{dt} - \frac{dn_2}{dt}\right) dt$$

where $\bar{t} = (t_1 + t_2)/2$ and $\Delta t = t_2 - t_1$ (the channel width) is small. This results in a contribution to the measured spectrum of

$$(4.28) \quad n(t) = n_0 \Delta t \exp-(\lambda_1^0 + K_{12})t + \frac{n_0 K_{12} \Delta t}{\lambda_2^0 - (\lambda_1^0 + K_{12})} \exp-(\lambda_1^0 + K_{12})t - \frac{n_0 K_{12} \Delta t}{\lambda_2^0 - (\lambda_1^0 + K_{12})} \exp-\lambda_2^0 t.$$

This expression contains two different observed annihilation rates, i.e. λ_2^0 and $\lambda_1^0 + K_{12}$. Referring to the previous section, the basis of this model is the assumption that the pickoff rate from the chemically bound state is significantly greater than the pickoff rate associated with the longest lived component, i.e. $\lambda_2 > \lambda_1 + K_{12}$. The result of this inequality is a predicted increase in I_3 relative to I_1 as opposed to the required decrease. (The first two terms in (4.28) are both positive, increasing the intensity of the long lived component.) This contradiction, as well as the presence of the exponential term in (4.28) with a negative intensity excludes the model as a possibility.

4.8 The "Conversion" Model

In the "conversion" model it is proposed that Ps undergoes conversion between the singlet and triplet states. It is assumed that this conversion might take place if there were a high enough concentration of paramagnetic ions in the positron spur. Since the analysis of this situation is similar to that of the "transition" model some of the details are omitted in the following development.

Schematically the above may be represented by the following diagram:

$$2\gamma \xleftarrow{\lambda_1^0} [n_1] \underset{K_{21}}{\overset{K_{12}}{\rightleftarrows}} [n_2] \xrightarrow{\lambda_2^p} 2\gamma$$

where $[n_1]$ is the population of o-Ps in the bubble, $[n_2]$ is the population of p-Ps in the bubble, $\lambda_1^0 = \lambda_{vac} + \lambda_p$, $\lambda_2^p = \lambda_0 + \lambda_p$ and $K_{21} = 3K_{12}$ (since there are 3 available states of o-Ps and one available state of p-Ps. Following Goldanskii[1B] the following differential equations may be written for this system:

$$(4.29) \quad \frac{dn_1}{dt} = (\lambda_1^0 + K)n_1 + 3K\, n_2$$

$$(4.30) \quad \frac{dn_2}{dt} = Kn_1 - (\lambda_2^p + 3K)n_2$$

where $K = K_{12}$. The eigenvalues of the system give the following exponential decay constants which may be interpreted as observed annihilation rates:

$$(4.31) \quad \Lambda_{1,2} = 1/2 \{(\lambda_1^0 + \lambda_2^p + 4K) \pm \sqrt{(\lambda_1^0 + \lambda_2^p + 4K)^2 - 4(\lambda_1^0 \lambda_2^p + 3K\lambda_1^0 + K\lambda_2^p)}\}$$

The state $[n_1]$ has a population 3/4F and the state $[n_2]$

has a population 1/4F at t = 0. The population of the two states will obey the relations

$$(4.32)\quad n_1(t) = \frac{3}{4}F\left\{\frac{\Lambda_2 - \lambda_1^0}{\Lambda_2 - \Lambda_1}\right\}\exp-\Lambda_1 t + \frac{3}{4}F\left\{\frac{\lambda_1^0 - \Lambda_1}{\Lambda_2 - \Lambda_1}\right\}\exp-\Lambda_2 t$$

$$(4.33)\quad n_2(t) = \frac{1}{4}F\left\{\frac{\Lambda_2 - \lambda_2^p}{\Lambda_2 - \Lambda_1}\right\}\exp-\Lambda_1 t + \frac{1}{4}F\left\{\frac{\lambda_2^p - \Lambda_1}{\Lambda_2 - \Lambda_1}\right\}\exp-\Lambda_2 t$$

where F is the fraction of positrons forming positronium and the populations $n_1(t) + n_2(t)$ are normalized to unity. This will result in a contribution to the lifetime spectrum which will be of the form

$$(4.34)\quad n(t) = \frac{1}{4}F\left\{\frac{4\Lambda_2 - \lambda_2^p - 3\lambda_1^0}{\Lambda_2 - \Lambda_1}\right\}\exp-\Lambda_1 t + \frac{1}{4}F\left\{\frac{3\lambda_1^0 + \lambda_2^p - 4\Lambda_1}{\Lambda_2 - \Lambda_1}\right\}\exp-\Lambda_2 t.$$

The low momentum component of the Doppler spectrum will be given by the portion of p-Ps not undergoing pickoff, or

$$(4.35)\quad I_A = \int_0^\infty \lambda_0 n_2 dt = \frac{1}{4}\frac{F\lambda_0}{\Lambda_1\Lambda_2}\left\{\frac{\Lambda_2(\Lambda_2 - \lambda_2^p) + \Lambda_1(\lambda_2^p - \Lambda_1)}{\Lambda_2 - \Lambda_1}\right\}.$$

The eigenvalue determinant used to solve for the $\Lambda_{1,2}$ may instead be used to solve for K so that

$$(4.36)\quad K = \frac{4\Lambda - 3\lambda_1^0 + \lambda_2^p}{\lambda_1^0\lambda_2^p - \Lambda\lambda_1^0 - \Lambda\lambda_2^p + \Lambda^2}$$

where both $\Lambda = \Lambda_1$ and $\Lambda = \Lambda_2$ must satisfy the expression. Some further manipulation will also give

$$(4.37)\quad \lambda_2^p = (\Lambda_1 + \Lambda_2) - \frac{4\Lambda_1\Lambda_2 I_A}{F}$$

and if it is assumed that I_1 of the lifetime spectrum contains all of the p-Ps annihilations then

$$(4.38) \quad \lambda_1^0 = \frac{4}{3} I_1 \frac{(\Lambda_2 - \Lambda_1)}{F} + \frac{4}{3}\Lambda_1 - \frac{1}{3}\lambda_2^p$$

Application of the foregoing relations to the experimental results would require the further relation

$$(4.39) \quad F = 1 - I_2$$

which assumes that I_2 contains all of the non-positronium annihilations. One may use these relations and the experimental data to calculate F, λ_2^p, λ_1^0, and then K using both the values Λ_1 and Λ_2 and comparing the two results. These calculations are given in table (4.9), showing a large discrepancy between the two calculated K values. Therefore, the results given in table (4.9) indicate that the "conversion" model does not hold.

TABLE 4.9

Calculated Results of the "Conversion" Model

SAMPLE	F	λ_2^p ($nsec^{-1}$)	λ_1^0 ($nsec^{-1}$)	K via Λ_1 ($nsec^{-1}$)	K via Λ_2 ($nsec^{-1}$)
BENZENE	0.666	4.43	1.50	0.24	4.85
HEXANE	0.633	4.23	1.47	0.17	3.96
2-METHYLPENTANE	0.635	4.21	1.28	0.21	3.93
3-METHYLPENTANE	0.660	4.15	1.38	0.23	4.87
2,2-DIMETHYLBUTANE	0.700	5.20	2.37	-0.10	3.92
2,3-DIMETHYLBUTANE	0.639	4.59	1.25	0.41	4.07
1-FLUOROHEXANE	0.480	3.48	2.21	-0.33	13.8
1-CHLOROHEXANE	0.420	3.17	2.05	-0.34	49.4

4.9 The "Branch" Model

The "branch" model assumes that some of the positronium formed does not enter the bubble state, but instead forms another state such as a bound state with a molecule or ion of the medium. (Incidentally, this model would apply equally well to the entry of some Ps atoms into an excited bubble state as opposed to the ground state in the normal case.) At time t = 0 let the fraction of positrons having formed positronium be F. At the same time let the fraction of F forming the bubble ground state be P. Schematically, the above could be represented by the following diagram for both o-Ps and p-Ps.

In this scheme let $\lambda_1^0 = \lambda_{vac} + \lambda_p$, $\lambda_1^p = \lambda_0 + \lambda_p$, $\lambda_2^0 = \lambda_{vac} + \lambda_B$ and $\lambda_2^p = \lambda_0 + \lambda_B$. The superscripts o and p refer to o-Ps and p-Ps, respectively and the subscripts 1 and 2 refer to the branches. λ_{vac} is the intrinsic vacuum annihilation rate of o-Ps, λ_0 is the intrinsic vacuum annihilation rate of p-Ps, λ_p is the pickoff rate in the bubble and λ_B is the pickoff rate in the bound state. The contribution to the lifetime spectrum due to Ps will then simply be

$$(4.40)\quad n(t) = \frac{3}{4}[F(1-P)]\exp-\lambda_2^0 t + \frac{1}{4}[F(1-P)]\exp-\lambda_2^p t + \frac{3}{4}FP\ \exp-\lambda_1^0 t + \frac{1}{4}FP\ \exp-\lambda_1^p t.$$

The intensity, I_A, of the low momentum component will be

$$(4.41)\quad I_A = \int_0^\infty \frac{\lambda_0}{4}\,[F(1-P)\exp-\lambda_2^p t + FP\ \exp-\lambda_1^p t]dt$$

$$= \frac{\lambda_0}{4}\left\{\frac{F(1-P)}{\lambda_2^p} + \frac{FP}{\lambda_1^p}\right\}.$$

These relationships may be tested as to their validity in describing experimental data.

As stated earlier, analysis of the experimental lifetime spectrum yields three distinguishable exponential components. It is assumed that λ_2^0, the o-Ps annihilation rate in the branch 2, is sufficiently great for this component to be unresolved computationally and appear mixed with the shortest lived component, I_1, and/or the intermediate component, I_2. Prediction of how much of the λ_2^0 component mixes into I_1 and how much mixes into I_2 is not possible. The limiting cases can however be considered, i.e. case I where the λ_2^0 component is totally contained in I_1 and case II where the λ_2^0 component is totally contained in I_2.

A qualitative consideration of the two cases may be useful. In Case I, I_1 is increased due to both o-Ps and p-Ps components from branch 2 and I_A' (the total amount of p-Ps) is increased due to the "extra" p-Ps from branch 2, agreeing with the experimentally observed relation (4.8), i.e. $I_1 > I_A' > I_3/3$. In case II both I_1 and I_A' are increased equally due to the p-Ps from branch 2, thus suggesting $I_1 = I_A' > I_3/3$. Assuming that, in the real case,

the situation is intermediate between case I and case II as suggested above, qualitatively, the model suggests $I_1 > I_A' > I_3/3$, in agreement with experimental results.

Quantitatively, using experimental values of I_1 and I_2 interpreted according to case I or case II assumptions and using experimental values of I_3, upper and lower limits for the predicted values of I_A may be calculated and compared with the experimental values.

For case I:

$$(4.42) \quad I_2 = 1 - F$$

$$(4.43) \quad I_1 = F(1 - P) + \frac{1}{4}FP \ .$$

For case II:

$$(4.44) \quad I_2 = 1 - F + \frac{3}{4}\{F\ (1 - P)\}$$

$$(4.45) \quad I_1 = \frac{1}{4}F(1 - P) + \frac{1}{4}FP \ .$$

For both cases:

$$(4.46) \quad I_3 = \frac{3}{4}FP$$

$$(4.47) \quad \lambda_3 = \lambda_1^0 \ .$$

The calculations of F, P and I_A for both cases are listed in table (4.10) along with the experimentally observed value of I_A. In four instances the calculated value of F for case II exceeds 1.0 so a limiting value of F = 1.0 is inserted. In three instances (benzene, 1-fluorohexane and 1-chlorohexane) case I alone describes the results within experimental error. For all the other samples the experimental value of I_A is bracketed by the extreme calculated values.

On the basis of the above results it may be concluded

TABLE 4.10

Calculations for the "Branch" Model

CASE I

SAMPLE	F	P	I_A (MIN.)	I_A (MEAS.)
BENZENE	0.67	0.78	0.15±0.01	0.14±0.01
HEXANE	0.63	0.86	0.14±0.01	0.18±0.02
2-METHYLPENTANE	0.64	0.89	0.15±0.01	0.19±0.02
3-METHYLPENTANE	0.66	0.86	0.15±0.01	0.17±0.02
2,2-DIMETHYLBUTANE	0.70	0.74	0.15±0.01	0.20±0.02
2,3-DIMETHYLBUTANE	0.64	0.90	0.15±0.01	0.17±0.02
1-FLUOROHEXANE	0.48	0.52	0.10±0.02	0.09±0.01
1-CHLOROHEXANE	0.42	0.44	0.09±0.06	0.05±0.01

CASE II

SAMPLE	F	P	I_A (MAX.)	I_A (MEAS.)
BENZENE	1.00	0.50	0.22	0.14±0.01
HEXANE	0.90	0.60	0.20	0.18±0.02
2-METHYLPENTANE	0.85	0.66	0.19	0.19±0.02
3-METHYLPENTANE	0.94	0.60	0.21	0.17±0.02
2,2-DIMETHYLBUTANE	1.00	0.52	0.22	0.20±0.02
2,3-DIMETHYLBUTANE	0.83	0.69	0.19	0.17±0.02
1-FLUOROHEXANE	1.00	0.25	0.21	0.09±0.01
1-CHLOROHEXANE	1.00	0.18	0.21	0.05±0.01

that of the three models considered to explain the relationships among the various intensities only the "branch" model adequately describes the experimental results. The implications of this result are that there is a second type of bound state for Ps besides the bubble ground state (in agreement with the prediction of the bubble model results) and that the amount of Ps formed is greater than the amount assumed to exist on the basis of the intensity of the long lived component.

The possibility that the Ps state in branch 2 is the 2s bubble state must be examined further. Comparison of P, the predicted fraction of Ps in the 1s bubble state, as given in table (4.7) and as given in table (4.10) for case I shows a very encouraging agreement especially in view of the approximation involved in the approach. Furthermore, the value of $k_1 R$ for the 2s state may also be used to calculate λ_B, the pickoff rate in the 2s state, according to equation (2.57). Performing this calculation yields, in each case, a value of $\lambda_2^0 = \lambda_{vac} + \lambda_B \simeq 1.2$ nsec^{-1} which falls between λ_3, the smallest observed pickoff rate or longest lifetime, and λ_2, the intermediate observed annihilation rate. A test of POSITRONFIT was performed in which a fourth component was incorporated into a generated hexane-like lifetime spectrum. This fourth component was given an intensity of 5% and an annihilation rate of 1 nsec^{-1} (a value lying between λ_2 and λ_3). POSITRONFIT failed to produce a four-

component result, instead giving a three-component result with most of the extra intensity from the 5% component going into I_1, and not, as expected, into I_2. This is consistent with the assumption of case I. Using λ_2^0 from above in place of the previously assumed limiting value it is reasonable to calculate the values of I_A predicted by case I of the branch model and compare them to the measured I_A values. These results are given in table (4.11) which shows reasonable agreement between the $I_A$values calculated and those measured, within the limits of uncertainty. For hexane and its isomers, however, the calculated I_A values are consistently below the measured values, by 0.02 or 0.03. This difference can be explained by the mixing of a small portion of the λ_2^0 component into I_2 instead of into I_1. The assumption that branch 2 of the branch model consists of 2s bubble states leads to a consistent description of the results and is therefore chosen to be the correct model based on the present evidence.

TABLE 4.11

The 2s Bubble State and the Branch Model

SAMPLE	F	P	I_A (CALC.)	I_A)MEAS.)
BENZENE	0.67	0.78	0.16±0.01	0.14±0.01
HEXANE	0.63	0.86	0.15±0.01	0.18±0.02
2-METHYLPENTANE	0.64	0.89	0.15±0.01	0.19±0.02
3-METHYLPENTANE	0.66	0.86	0.16±0.01	0.17±0.02
2,2-DIMETHYLBUTANE	0.70	0.74	0.17±0.01	0.20±0.02
2,3-DIMETHYLBUTANE	0.64	0.90	0.15±0.01	0.17±0.02
1-FLUOROHEXANE	0.48	0.52	0.11±0.02	0.09±0.01
1-CHLOROHEXANE	0.42	0.44	0.10±0.06	0.05±0.01

4.10 Conclusion

This work has produced significant results in three areas. First, since the Doppler technique and the DOPPFIT computer program have not previously been used in the study of positrons in liquids, this work establishes the usefulness of the more efficient Doppler method as compared to the angular correlation method. Second, the success of the bubble model in describing the low momentum Doppler component and the long lived lifetime component is demonstrated. The bubble model results predict the presence of a second type of bound state (probably an excited bubble state) not previously observed by experimenters in these liquids. Finally, the branch model is demonstrated to be the only model of those considered which adequately describes the relationships among the various intensities. This model is shown to predict a second state, reinforcing the identical prediction of the bubble model.

REFERENCES

1. V.I. Goldanskii, Atomic Energy Review 6, 3 (1968).

1A. V.I. Goldanskii, in Reference 1, p. 28.

1B. V.I. Goldanskii, in Reference 1, p. 130.

2. S. Cova and L. Zappa, J. Phys. B. 1, 795 (1968).

3. A. Ore, Univ. of Bergen, Arbok Naturvitenskap, Rekke 9, (1949).

4. O. E. Mogensen, J. Chem. Phys. 60, 998 (1974)

5. P.R. Gray, C.F. Cook and G. P. Sturm Jr., J. Chem. Phys. 48, 1145 (1968).

6. S.J. Tao, J. Chem. Phys. 56, 5499 (1972).

7. A. Bisi, G. Gambarini and L. Zappa, Il Nuovo Cimento 67B, 75 (1970).

8. U. Brandt, S. Berko and W.W. Walker, Phys. Rev. 120, 1289 (1960).

9. A. P. Buchikhin, V. I. Goldanskii, A. O. Tatur and V. P. Shantarovich, Soviet Physics JETP 33, 615 (1971).

10. S. Dannefaer and D.P. Kerr, Nuc. Instr. Methods 131, 119 (1975).

11. R. A. Ferrel, Phys. Rev. 108, 167 (1957).

12. L. O. Roellig and T. M. Kelly, Phys. Rev. Letters 18, 387 (1967).

13. K. F. Canter, Ph.D. Thesis, Wayne State University, p. 13, 1970 (unpublished).

14. E. Merzbacher, Quantum Mechanics (Wiley, 1961), p. 412.

15. D. R. Bates, ed., Quantum Theory (Academic, 1961), p. 106.

16. G. Baym, Lectures on Quantum Mechanics (Benjamin, 1973), p. 161.

17. S. Flügge, Practical Quantum Mechanics I (Springer-Verlag, 1973), pp. 200, ff.

18. A. T. Stewart, Can. J. Phys. 35, 168 (1957).

19. C. V. Briscoe, S. I. Choi and A. T. Stewart, Phys. Rev. Letters 20, 493 (1968)

20. R. C. Tolman, J. Chem. Phys. 17, 323 (1949).

21. P. Kirkegaard and M. Eldrup, Comp. Phys. Comm. 3 240 (1972).

22. P. Kirkegaard and M. Eldrup (unpublished).

23. L. E. Spanel, A. S. Rupaal and J. R. Patrick, Phys. Rev. B 8, 4072 (1973).

24. S. Dannefaer, private communication.

25. J. Lee and G. J. Celitans, J. Chem. Phys. 42, 437 (1965).

26. D. P. Kerr, A. M. Cooper and B. G. Hoog, Can. J. Phys. 43, 963 (1965).

27. V. I. Goldanskii and V. P. Shantarovich Appl. Phys. 3, 335 (1974).

28. S. Sugden, J. Amer. Chem. Soc. 70, 1483 (1921).

29. O. E. Mogensen, private communication.

30. D. P. Kerr, Ph. D. Thesis, University of Manitoba, 1964 (unpublished).

31. G. Deblonde, S. Y. Chuang, B. G. Hogg, D. P. Kerr and D. M. Miller, Can. J. Phys. 50, 1619 (1972).

32. J. P. Hernandez and S. I. Choi, Phys. Rev. 188, 340 (1969).

33. R. N. West, Positron Studies of Condensed Matter (Taylor & Francis, 1974), pp. 71 - 75.

33A. R. N. West, in Reference 33, p. 14.

34. J. D. McGervey, Positron Annihilation, edited by A. T. Stewart and L. Roellig, (Academic Press, 1967), p. 143.

APPENDIX I

A TEST SPECTRUM GENERATING COMPUTER PROGRAM

This program calculates a simulated 512 channel lifetime spectrum and places it on magnetic disc where it may be accessed by POSITRONFIT. The following are the input parameters.

AREA, IC, IX, SENS, ZERO, NRES
FØRMAT (F9.0, IX, I1, 1X, F1, 1X, F6.5, 1X, F6.2, 1X, I2)

where IC is the number of exponential components, IX = 0 results in no generated statistics, IX = 1,3, ... etc. results in generated statistics, SENS is the spectrum calibration in nsec/channel, ZERO is the zero time channel number and NRES is the number of points in the input resolution spectrum.

CT(I), CI(I), I = 1,IC
FØRMAT (F5.3, 1X, F6.5)

where CT(I) are the component lifetimes in nsec and CI(I) are the component intensities expressed as decimal fractions and entered in pairs of CT(I) and CI(I) values.

RES(NRES-I+1), I = 1,NRES)
FØRMAT (8F8.0)

where RES is the experimental resolution spectrum read in inverted order by the computer.

The output indicates whether statistics are generated or not, prints out the input parameters and the generated spectrum.

```
      INTEGER IC,IX,N,IDATA(512)
      REAL DATA(550),AREA,SENS,ZERO,CI(7),CT(7)
      DO 100 I=1,550
  100 DATA (I)=0.
      READ(5,10) AREA,IC,IX,SENS,ZERO,NRES
      READ(5,15)(CT(I),CI(I),I=1,IC)
      WRITE(6,20)
      WRITE(6,25)(CT(I),I=1,IC)
      WRITE(6,30)(CT(I),I=I,IC)
      WRITE(6,35)AREA,SENS,ZERO
      IF(IX.NE.0)WRITE(6,60)
      IF(IX.EQ.0)WRITE(6,55)
      DO 105 J=1,IC
  105 CI(J)=CI(J)*AREA
      IZERO=IFIX(ZERO+.5)
      T2=SENS*(IZERO-ZERO+.5)
      DO 110 J=1,IC
  110 DATA(IZERO)=DATA(IZERO)+CI(J)*(1.-EXP(-T2/CT(J)))
      N=IZERO+1
      DO 125 I=N,550
      T1=SENS*(I-ZERO-.5)
      T2=SENS*(I-ZERO+.5)
      DO 125 J=1,IC
  125 DATA(I)=DATA(I)+CI(J)*(EXP(-T1/CT(J))-EXP(-T2/CT(J)))
      CALL FOLD(DATA,NRES)
      DO 120 I=1,550
  120 DATA(I)=DATA(I)+100.
      IF(IX.EQ.0)GOTO126
      DO 130 I=1,512
      CALL GAUSS (IX,SQRT(DATA(I)),DATA(I),DATA(I))
  130 IDATA(I)=IFIX(DATA(I)+.5)
  126 CONTINUE
      WRITE(6,40)
      WRITE(6,45)(DATA(I),I=1,512)
      WRITE(8,50)(IDATA(I),I=1,512)
   10 FORMAT(F9.0,1X,I1,1X,I1,1X,F6,5,1X,F6.2,1X,12)
   15 FORMAT(F5.3,1X,F6.5)
   20 FORMAT('1','INPUT TO DATA GENERATOR')
   25 FORMAT(/,' LIFETIMES =',(7F8.3))
   30 FORMAT(/,' INTENSITIES =',(7F8.5))
   35 FORMAT(/,' AREA =',F9.0,5X,'SENSITIVITY =',F7.5,5X,'ZERO =',F6.2)
   40 FORMAT(/,' GENERATED DATA',/)
   45 FORMAT(1X,8F10.2)
   50 FORMAT(8(16,1X))
   55 FORMAT(/,' ****STATISTICS NOT USED****')
   60 FORMAT(/' ****STATISTICS USED****')
      STOP
      END
      SUBROUTINE FOLD(DATA,NRES)
      REAL DATA(550),RES(100),DATA2(550)
      INTEGER NR
      READ(5,55)(RES(NRES-I+1),I=1,NRES)
   55 FORMAT(8F8.0)
      RMAX=RES(1)
```

```
      AREA=0.0
      DO 135 I=1,NRES
      AREA=AREA+RES(I)
      IF(RES(I)-RMAX)135,140,140
  140 RMAX=RES(I)
      NR=I
  135 CONTINUE
      DO 150 I=1,NRES
  150 RES(I)=RES(I)/AREA
      DO 145 I=1,550
      DATA2(I)=0.
      DO 145 JJ=1,NRES
      J=I-NR+JJ
      IF(J.GE.1.AND.J.LE.550) DATA2(I)=DATA2(I)+RES(JJ)*DATA(J)
  145 CONTINUE
      DO 155 I=1,550
  155 DATA (I)=DATA2(I)
      RETURN
      END
      SUBROUTINE GAUSS(IX,S,AM,V)
      A=0.0
      DO 150 I=1,48
      CALL RANDU(IX,IY,Y)
      IX=IY
  150 A=A+Y
      V=(A-24.)*S/2.+AM
      RETURN
      END
      SUBROUTINE RANDU(IX,IY,YFL)
      IY=IX*65539
      IF(IY)155,160,160
  155 IY=IY+2147433647+1
  160 YFL=IY
      YFL=YFL*.4656613E-9
      RETURN
      END
$ENTRY
```

Two representative tests of the modified POSITRONFIT using the above described spectrum generating program are listed in the following table. The standard deviations listed are those calculated by POSITRONFIT. The results are accurate to within the standard deviations in all of the cases except for the shortest lifetime in each test where the results are still reasonably close.

CASE I

INPUT

Lifetime (nsec)	3.926	0.548	0.232
Intensity (%)	39.56	29.63	30.81

OUTPUT

Lifetime (nsec)	3.926	0.553	0.239
std. dev.	0.008	0.011	0.005
Intensity (%)	39.75	29.22	31.03
std. dev.	0.09	1.15	1.20

CASE II

INPUT

Lifetime (nsec)	2.680	1.330	0.350
Intensity (%)	14.10	9.90	76.00

OUTPUT

Lifetime (nsec)	2.659	1.359	0.355
std. dev.	0.054	0.089	0.001
Intensity (%)	14.28	9.47	76.26
std. dev.	1.04	0.83	0.30

APPENDIX II

A LEAST SQUARES FIT COMPUTER PROGRAM

```
C
C THIS PROGRAM PERFORMS A LEAST SQUARE FIT OF THE MOMENTUM DISTRIBUTION
C CALCULATED FROM THE BUBBLE MODEL POSITRONIUM WAVE FUNCTION TO THE
C MOMENTUM DISTRIBUTION OBTAINED FROM A GAUSSIAN FIT TO THE NARROW
C COMPONENT OF THE DECONVULTED DOPPLER SPECTRUM.
C
      REAL*8 SIGMA,R,K,KR,K1R,A,B,R1,K1R1,KL,KI,TST,VARM(2),FIT(20),TABL
     1E(20),VAR(20,20),DEXP,DSIN,DCOS,DCOT,PHI,GAUSS,AF,AT
      INTEGER L
C
C INPUT SIGMA IN KEV, GUESSED R IN ANGSTOMS,GUESSED K1R, AND
C THE FITTING REGION, KL IN MOMENTUM UNITS (1/CM) TIMES R, AND
C THE VARIATION PARAMETER FOR R AND K1R (1 = 10 PERCENT, 2 = 1 PERCENT)
C     READ(5,100) SIGMA,R,K1R,KL,L;WRITE (6.150) SIGMA,R,K1R,KL
      IF(L.EQ.1)GOTO5;WRITE(6,160);GOTO6
    5 WRITE(6,170)
    6 CONTINUE
C
C CONVERT SIGMA TO MOMENTUM UNITES (1/CM) AND R TO CM
C
      SIGMA=SIGMA*1.01353623ID 08;R=R*1.D-08
C
C DEFINE NORMALIZATION CONSTANTS FOR THE TWO MOMENTUM DISTRIBUTIONS,
C A FOR FIT AND B FOR TABLE.
C
      DATA A/1.128379167D 03/,B/2.256758334D 06/
C
C CALCULATE TABLE VALUES FROM GAUSSIAN FIT TO NARROW PART OF
C DECONVOLUTED DOPPLER SPECTRUM.
C
      K1=KL/9.D-7;K=KI;AT=0.;DO 1 1=1,20;TABLE (1)=GAUSS (K,SIGMA,B)
      AT=AT+TABLE(I)*KI
    1 K=K+KI
C
C INCREMENT R AND K1R IN 20 STEPS ABOUT GUESSED VALUES AND FORM A 20×20
C MATRIX OF VARIANCES.  FIND VALUES GIVING LOWEST VARIANCE BETWEEN FIT
C AND TABLE AND REPLACE R AND K1R BY THESE.  REPEAT PROCEDURE USING
C FINER STEPS OF R AND KR.
C
      K1R1=K1R;R1=R;K1R=K1R1-.1*K1R1/(10.**(L-1))
      D040J=1,20;R=R1-.1*R1/(10.**(L-1));DO3OKC=1,20;K=K1;AF=0.
      DO 10KF=1,20;KR=K*R;FIT(KF)=PHI(R,KR,K1R,A)**2
      AF=AF+FIT(KF)*KI
   10 K=K+KI;VAR(J,KC)=0.;DO 20 KV=1,20
   20 VAR(J,KC)=VAR(J,KC)+(FIT(KV)*AT/AF-TABLE(KV))**2
   30 R=R+.01*R1/10.**(L-1))
   40 K1R=K1R+.01*K1R1/(10.**(L-1));;WRITE(6,110)((VAR(J,KK),KK=1,20),J=
     11,20)
      TST=1.D 50;DO 50 J=1,20;DO 50 KK=1,20;IF(VAR(J,KK).GE.TST)GOT050
      TST=VAR(J,KK):VARM(1)=J;VARM(2)=KK
   50 CONTINUE
      K1R1=K1R1-(.11-VARM(1)*.01)*K1R1/(10.**(L-1))
      R1=R1-(.11-VARM(2)*.01)*R1/(10.**(L-1));WRITE(6,120)K1R1,R1*1.D8
```

```
  100 FORMAT(4F6.3,12)
  110 FORMAT(IX,10E12.4/1X,10E12.4/)
  120 FORMAT(' ',' BEST K1R VALUE = ',F7.4,'  BEST R VALUE = ',F7.4,'ANG
     1STROMS')
  150 FORMAT('1',' INPUT SIGMA = ',F6.3,' KEV.  GUESSED R = ',F6.3,' ANG
     1STROMS.  GUESSED K1R = ',F6.3/' FITTING REGION = ',F6.3)
  160 FORMAT (' FIT CALCULATED TO .1 PERCENT ACCURACY.')
  170 FORMAT (' FIT CALCULATED TO 1 PERCENT ACCURACY.')
      STOP;END
C
      REAL FUNCTION GAUSS*B(K,SIGMA,B);REAL*8 K,SIGMA,B,DEXP
      GAUSS=B/SIGMA**3*K**2*DEXP(-K**2/SIGMA**2);RETURN;END
C
      REAL FUNCTION DCOT*8(X)
      REAL*8 X,DCOS,DSIN;DCOT=DCOS(X)/DSIN(X);RETURN;END
C
      REAL FUNCTION PHI*8 (R,KR,K1R,A)
      REAL*8 R,KR,K1R,DCOT,DSIN,DCOS,DCSC,A
      PHI=A*R**.5*(K1R*DCOT(K1R)/(K1R*DCOT(K1R)-1.))**.5*(K1R/DSIN(
     1K1R))**2/(K1R**2-KR**2)*(KR*DSIN(K1R)*DCOS(KR)-K1R*DCOS(K1R)*DS
     2IN(KR)) / ((K1R*DCOT(K1R))**2*KR**2);RETURN;END
```

APPENDIX III

THE BISECTION METHOD

Suppose that an equation, f(x) = 0, is negative at x = a and positive at x = b. If f [(a+b)/2] is calculated and if it is zero then we have the required root. If f [(a+b)/2] is negative, then the root is between (a+b)/2 and b. If it is positive, the root is between (a+b)/2 and a. Thus, either we have the root or we have bracketed it within an interval half as large as the previous one. This process can be continued, each time bisecting the interval, until the root is known to the desired accuracy.

FLOW CHART